# Lithospheric structuration onshore-offshore of the Sergipe-Alagoas passive margin, NE Brazil, based on wide-angle seismic data

J.M. Pinheiro, P. Schnürle, M. Evain, A. Afilhado, F. Gallais, F. Klingelhoefer, A. Loureiro, R. Fuck, J. Soares, A. Cupertino, et al.

# Lithospheric structuration onshore-offshore of the Sergipe-Alagoas passive margin, NE Brazil, based on wide-angle seismic data ☆

Pinheiro Joao Marcelo [1, *], Schnurle Philippe [1], Evain Mikael [1], Afilhado A. [2], Gallais Flora [1], Klingelhoefer Frauke [1], Loureiro Afonso [3], Fuck R. [4], Soares J. [4], Cupertino J.A. [5], Viana A. [5], Rabineau Marina [6], Baltzer Agnes [7], Benabdellouahed Massinissa [6], Dias N. [2, 3], Moulin Maryline [1], Aslanian Daniel [1], Morvan Laetitia [8], Mazé Jean-Pierre [8], Pierre Delphine [8], Roudaut-Pitel M. [8], Rio I. [9], Alves D. [9], Barros Junior P. [11], Biari Youssef [8], Corela C. [9], Crozon Jacques [8], Duarte J.L. [9], Ducatel Cecile [8], Falcão C. [11], Fernagu Philippe [8], Le Piver David [8], Mokeddem Zohra [10], Pelleau Pascal [8], Rigoti C. [11], Roest Walter [8], Roudaut Mickael [8]

[1] Institut Français de Recherche pour l'Exploitation de la MER, IFREMER, REM/GM, Centre de Brest, 29280, Plouzané, France
[2] Instituto Superior de Engenharia de Lisboa, ISEL, Instituto Politécnico de Lisboa, R. Conselheiro Emídio Navarro, 1959-007, Lisbon, Portugal
[3] Instituto Dom Luiz, Faculdade de Ciências, Universidade de Lisboa, Campo Grande, Ed. C1, Piso 1, 1749-016, Lisbon, Portugal
[4] Instituto de Geociências, Universidade de Brasília, Campus Darcy Ribeiro, 70910-900, Brasilia, Brazil
[5] Petrobras, Cenpes Research Center, Rio de Janeiro, Brazil
[6] Laboratoire Géosciences Océan, UMR6538, Université de Bretagne Occidentale, Place Nicolas Copernic, 29280, Plouzané, France
[7] Géolittomer, LETG UMR 6554-CNRS, Institut de Géographie et d'Aménagement Régional de l'Université de Nantes, Campus Tertre, BP 81227, 44312, Nantes, CEDEX 3, France
[8] Institut Français de Recherche pour l'Exploitation de la MER, IFREMER, REM/GM, Centre de Brest, 29280, Plouzané, France
[9] Instituto Dom Luiz, Faculdade de Ciências, Universidade de Lisboa, Campo Grande, Ed. C1, Piso 1, 1749-016, Lisbon, Portugal
[10] Laboratoire Géosciences Océan, UMR6538, Université de Bretagne Occidentale, Place Nicolas Copernic, 29280, Plouzané, France
[11] Géolittomer, LETG UMR 6554-CNRS, Institut de Géographie et d'Aménagement Régional de l'Université de Nantes, Campus Tertre, BP 81227, 44312, Nantes, CEDEX 3, France

* Corresponding author : Joao Marcelo Pinheiro, email address : jmpgeo@gmail.com

**Abstract :**

The structure and nature of the crust underlying the Camamu-Almada-Jequitinhonha-Sergipe-Alagoas basins System, in the NE Brazilian margin, were investigated based on the interpretation of 12 wide-

angle seismic profiles acquired during the SALSA (Sergipe ALagoas Seismic Acquisition) experiment in 2014. In this work, we present two 220-km-long NW-SE combined wide-angle and reflection seismic profiles, SL 01 and SL 02, that have been acquired using 15 ocean-bottom-seismometers along each profile, offshore the southern part of the Sergipe Alagoas Basin (SAB), north of the Vaza-Barris Transfer zone. The SL 02 has a 150-km long inland continuation with 20 land-seismic-stations until the Sergipano Fold Belt (SFB). Wide-angle seismic forward modeling allows us to precisely divide the crust in three domains: beneath the continental shelf, a ~100 km wide necking zone is imaged where the continental crust thins from ~35 km on the Unthinned Continental Domain, which displays a three-layered crust structure, to less than 8 km on the Oceanic Crust Domain. In the necking zone, the upper and the middle layers thin dramatically and almost disappear, while the Moho discontinuity shows clear PmPs. The Continental-Oceanic Crust Boundary (COB) is located at ~80 km from the coastline and is marked by intracrustal seismic reflectors and changes in the seismic velocity, showing a sharp transition. On profile SL02, the oceanic crust is perturbed by a volcanic edifice together with an anomalous velocity zone underneath the area.

**Highlights**

► Sergipe Alagoas Basin passive margin modeling. ► Wide-angle refraction seismic integrated with Multi-Channel reflection seismic data. ► Location of the Continental- Oceanic crust boundary. ► Lithospheric structuration and segmentation of Brazil's margin in Central Atlantic.

## Introduction

Understanding the processes that led to the breakup of West Gondwana (Figure 1A) and the formation of the south Atlantic Margins are still not fully achieved. The North – East Brazilian margins, which are very segmented margins, in various structural and inheritance contexts, where the aborted Recôncavo - Tucano - Jatoba rift system connects with the NS Jequitinhonha - Camamu-Almada and NE-SW Jacuípe - Sergipe-Alagoas rift systems are a strategic area to study the influence of the tectonic inheritance on margin's formation. The connection between the three system forms the Camamu triple junction. The SALSA experiment, conducted in 2014 by the Department of Marine Geosciences (IFREMER: Institut Français de Recherche pour l'Exploitation de la MER, France) and PETROBRAS (Brazil), in collaboration with the Laboratory of Oceanic Domain (IUEM: Institut Universitaire et Européen de la Mer, France), the Faculdade de Ciências da Universidade de Lisboa (IDL, Portugal) and the Universidade de Brasilia (Brazil), is aimed at constraining the crustal structure, the segmentation and the geodynamical setting of the Jequitinhonha-Almada-Camamu-Jacuípe-Alagoas-Sergipe margin segments.

In the year 2000's high quality seismic profiles from ION-GXT were acquired off Brazil's coast, and a few of these profiles have been published, particularly in the Brazilian southeastern margin (e.g., Henry *et al*., 2009; Kumar *et al*., 2012). The location of the SALSA profiles follows the location of some of the ION-GXT profiles. Seismic shots, Multi-Channel Seismic (MCS) acquisition and Ocean Bottom Seismometers (OBS) deployments were performed by the French R/V L'Atalante (IFREMER) along twelve profiles (Figure 1B). Among them, five were extended onshore by Land Seismic Stations (LSS). Here, we present the results on P-wave velocity models, based on the combined interpretation of multi-channel and wide-angle seismic data, of two profiles imaging the Sergipe-Alagoas basin (SAB), located in the northern part of the experiment, north to the Vaza-Barris transfer zone (Figures 1C and 2). The remaining basins studied during the SALSA project (Camamu (Loureiro *et al.*, 2018), Jacuípe, Tucano and Sergipe-Alagoas basins) will be discussed in companion papers.

2

67
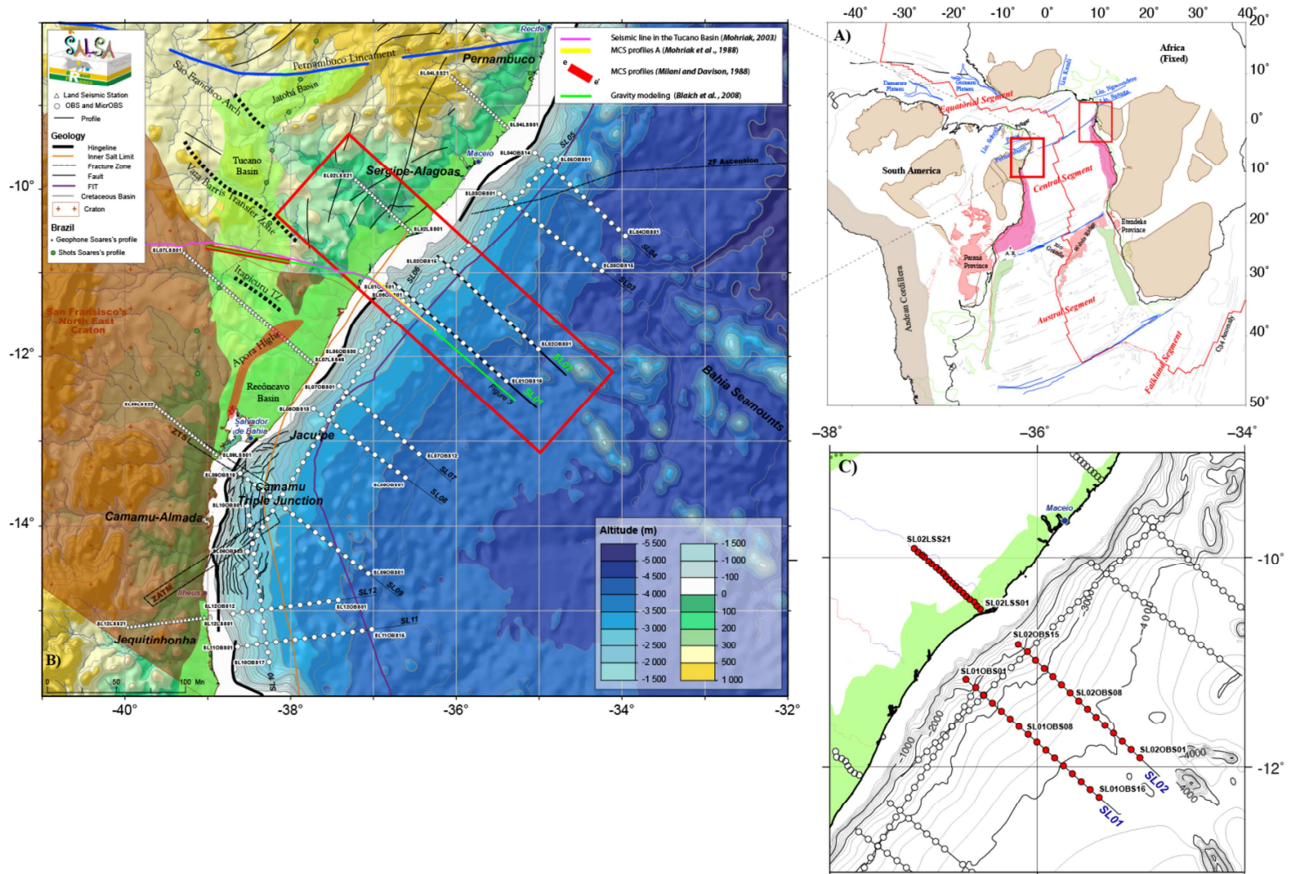


68 *Figure 1: Location of profiles of the SALSA experiment: A) General reconstruction map at Chron C34 of studied area*
69 *and conjugate margin (Moulin et al., 2010). B) Bathymetry and topography on land (IHO-IOC GEBCO, 2014). Ocean*
70 *Bottom Seismometers (OBSs) are marked by white dots, MCS profiles by thick black lines, land-stations by white*
71 *triangles. The SL01 and SL02 profiles are highlighted by red rectangle. The color lines represent the location of*
72 *profiles already published in this area. Dashed black line denotes main transfer zones (Blaich et al., 2008). Green area*
73 *indicates the Recôncavo-Tucano-Jatoba (RTJ) basins (Bizzi et al., 2003). Brown area indicates the limits of the Sao*
74 *Francisco Craton, adapted from Hasui (2012). TMAZ: Taipus-Mirim Accommodation Zone. Note that Bahia Seamounts*
75 *are characterized by an elongated NW-SE direction. C) Bathymetry (IHO-IOC GEBCO, 2014) around the profiles*
76 *discussed in the present paper.*
77

## Geological Setting

79  Whilst in Albian time the central part of the South Atlantic presented the first oceanic crust, the

80  Equatorial Atlantic Ocean was only starting to open, as the last stage of the breakup of the Atlantic

81  Ocean, allowing the definitive water connection between the Central Atlantic and the South Atlantic

82  oceans (Moulin *et al.,* 2010). From the Potiguar Basin to the north to the Camamu triple junction to

83  the south (figure 1A), this area represents a buffer zone between these two different geodynamical

84  settings (Conceiçao and Zalan, 1998; Moulin *et al.,* 2010).

85  This buffer zone is characterized by a SW-NE elongated margin, oblique respect to the main

86  direction of the Fracture zones of the central segment of the South Atlantic Ocean. Onshore the

87  presence of a failed N-S and E-W rift: the Recôncavo-Tucano-Jatoba rift, marks the limit of the

88  Triangle-shaped Tucano Microplate, which rotated counterclockwise (Szatmari *et al.,* 1999; Moulin

89  *et al.,* 2010) during the South Atlantic opening. The Sergipe Alagoas Basin (SAB) is situated in the

3

90   middle of the eastern branch of this triangle, to the north of the Vaza-Barris Fault, which marks the

91   boundary between the Sergipe basin and Jacuipe basin depocenters. It is in the east of the Sergipano

92   Fold Belt (SFB) and south of the Pernambuco lineament, which are geological structures associated

93   with the tectonic development of NE Brazil (Figure 2), inherited from the Neoproterozoic

94   Brasiliano Orogeny (Davison *et al*., 1995). The role of the Vaza-Barris transfer zone, is not yet

95   completely understood, but it plays a significant role in the actual framework of the Brazilian

96   margin, as it divides the Tucano basin and produces a flip in the location of its depocenters.

97   Stratigraphically, the SAB is one of the few basins that presents Paleozoic to Jurassic/Early

98   Cretaceous pre-rift sequences related to intracratonic subsidence and is the northern limit of the

99   evaporite deposits (Cainelli and Mohriak, 1998).

100   Sediments in the SAB lie over the Proterozoic SFB (Figure 2). The SFB is located between the

101   Pernambuco-Alagoas Massif and the São Francisco Craton (SFC) (Figures 1 and 2) with a

102   triangular shape narrowing towards the west (Figure 2). The geological history of the SFB has been

103   the subject of numerous studies (e.g. Almeida *et al.,* 1977; Davison and Santos, 1989; D'el-Rey

104   Silva, 1999). Recently Oliveira *et al.* (2010), based on U–Pb SHRIMP (Sensitive High-Resolution

105   Ion Microprobe) and detrital zircons ages from Carvalho *et al.* (2005), proposed that the evolution

106   of the Sergipano Belt began with the breakup of a Palaeoproterozoic continent followed by

107   development of a Mesoproterozoic (≈980–960 Ma) continental arc possibly on the margin of the

108   Palaeoproterozoic Pernambuco-Alagoas Massif. The extension of this continental block resulted in

109   a stretched margin, a passive margin on the southern edge of the Pernambuco-Alagoas Massif with

110   a rift in between. A second passive margin was formed on the São Francisco Craton. Convergence

111   of the Pernambuco-Alagoas Massif and the São Francisco Craton led to deformation in shelf

112   sediments, build-up of a continental arc between 630 Ma and 620 Ma, and subsequent exhumation

113   and erosion of the Pernambuco-Alagoas Block, led to deposition of the uppermost Pre-Cambrian

114   clastic sediments (Oliveira *et al.,* 2010).

115   The SAB presents a complete rift stratigraphic record (Mohriak, 2003). The initial rift deposits

116   records can be observed in the onshore part of the SAB.  Gomes (2005), using well logs information

117   with seismic data (Cainelli, 1992), had tracked continuous seismic horizons related to the base of

118   the Calumbi Formation, which marks the beginning of the drift phase. Campos Neto *et al.* (2007)

119   elaborated the Petrobras stratigraphic chart, following the lithostratigraphic classification proposed

120   by Schaller (1970) and Feijó (1994).

121   Mohriak *et al.* (1995, 1998, 2000) and Mohriak (2003) interpreted the regional seismic section 238-

122   RL-343 (Figures 1 and 3). This profile is perpendicular to the coast and hinge line and extends for

123   about 110 km from the platform to the deep water-region of the SAB. He did an interpretation

124 stratigraphically calibrated by exploration boreholes and structurally constrained by gravity
125 modelling. The results of a deep geoseismic transect were also used by Blaich *et al.* (2008, 2011) to
126 model the crust of the SAB in combination of new gravity data. From these past studies, we can
127 assume some key elements:

128 • Mohriak *et al*. (1998) described a conspicuous array of strong undulated reflectors in the
129 lower portion of the profile (Figure 3) forming an anticlinal structure that rises from the
130 westernmost portion of the profile until the apex near the shelf-break and extends as a band of
131 reflectors throughout most of the profile (Figure 3), from slope to deep basin. He suggested that
132 they might correspond to intracrustal horizons that probably mark the transition from the lower
133 crust to the upper mantle ultramafic rocks (Kemplerer *et al*., 1986).

134 • Mohriak *et al*. (1998) observed some structures in the proximal deep-water basin that was
135 interpreted as igneous bodies (Figure 3). One example is a plug interpreted as a post-rift volcanic
136 intrusion close to the Continental Ocean Boundary (COB) (Figure 3). Bordering this plug, in the
137 proximal side, there are packages of reflectors with a sigmoidal geometry, mostly dipping seawards,
138 but also dipping landwards, that probably correspond to seaward-dipping-reflectors and landward
139 dipping reflectors (SDRs and LDRs) (Figure 3), which were interpreted as formed by volcanic
140 rocks extruded during early phases of spreading oceanic ridges (Mohriak *et al*., 1998). These
141 magmatic features are usually associated with extensional processes and oceanic crust inception,
142 and therefore post-date the rift-phase lithospheric extension associated with the break-up of
143 Gondwana in the Early Cretaceous. On the base of this observations, Mohriak *et al.* (1995)
144 suggested that the central segment of the South Atlantic African margins could also be considered
145 as a volcanic margin such as the Norwegian margin (e.g. Eldholm *et al.,* 1989), the Greenland
146 margin (e. g. Korenaga *et al.,* 2000), the Aden margin (Tard *et al.*, 1991) or the Namibia margin
147 (Bauer *et al.,* 2000; Austin and Uchupi, 1982). However, Moulin *et al.* (2005) have quoted the
148 differences between the 4 km thick SDRs layer lying on top of a 30km-thick igneous crust and
149 extending over a lateral distance of 150km on the Greenland margin (Korenaga *et al.,* 2000) and
150 this less than 20km wide and less than 3km thick SDRs described by Mohriak *et al.* (1995). They
151 argued that if their thickness is similar, their lateral extensions are quite different and the same
152 genetic process can hardly be attributed to both structures.

153 • Assuming a simple geologic model based in thinning of the crust with mantle rising from 35
154 km in the onshore region to about 25 km at the platform, and to about 20 km near the shelf edge, the
155 gravity modelling for the Sergipe sub-basin and the Jacuipe Basin suggests a very rapid crustal
156 thinning near the present-day shelf edge (Mohriak *et al.*, 1995, 1998). According to this modelling,
157 the Moho topography gets more regular from slope to seawards with depths between 15 and 18 km
158 across the COB (Figure 3).

5

159  •      In addition to the rapid shallowing of the Moho and the presence of SDRs, the 2D gravity
160  modeling of Blaich *et al.* (2008) required the introduction of a lower crustal high-density body in
161  the proximal part of the gravimetric profile, in the necking zone, between 200 km and 300 km
162  distance (Figure 4). For these authors this high-density body would indicate a volcanic margin
163  character.

164  •      The COB location was evaluated by this 2D gravity modelling (Blaich *et al.,* 2008) and
165  illustrates also a Moho discontinuity that shallows very rapidly eastward of the depocenter, rising
166  from 33 km to 18 km depth within a distance of about 70 km, not so different of the model
167  proposed by Mohriak *et al.* (1998).

168
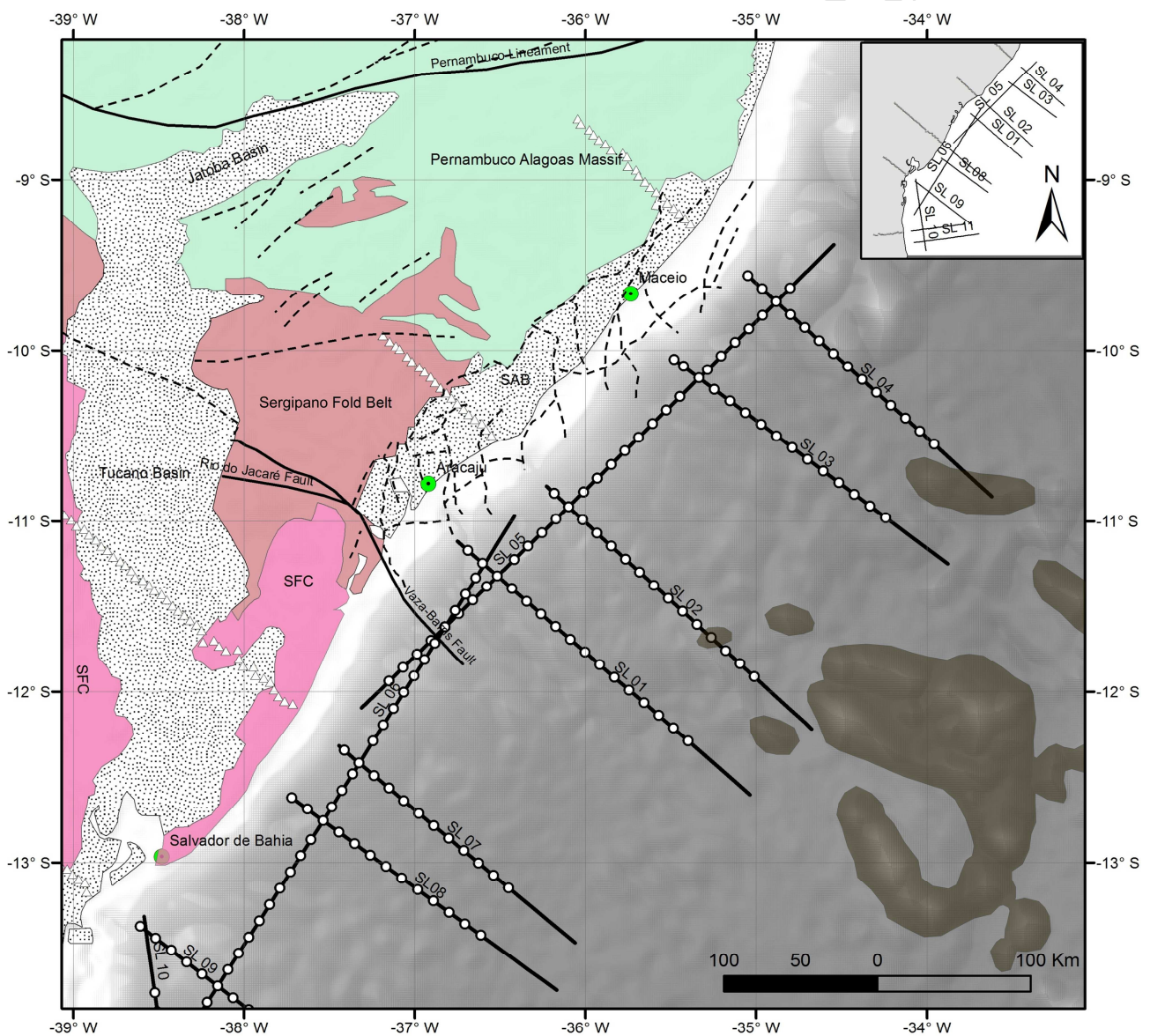


**Legend**

△ Land Seismic Stations (LSS)

○ Ocean Bottom Seismometer (OBS)

— Salsa profiles

**Structures**

- - - - Fractures and faults

—— Principal lineaments and zones of transference

**Geology**

Cretaceous basins

Proterozoic orogenic belts

Palaeoproterozoic Borborema Province

Palaeoproterozoic São Francisco Craton

Bahia Seamounts

169

170 *Figure 2. Geological Map of the Basin Sergipe-Alagoas and region around (modified from Lana, 1990,) with the*
171 *SALSA profiles, the principal faults and fractures, and the geological features associated with the São Francisco*
172 *Craton (SFC), the SFB and the Sergipe Alagoas Basin (SAB). Mercator projection.*
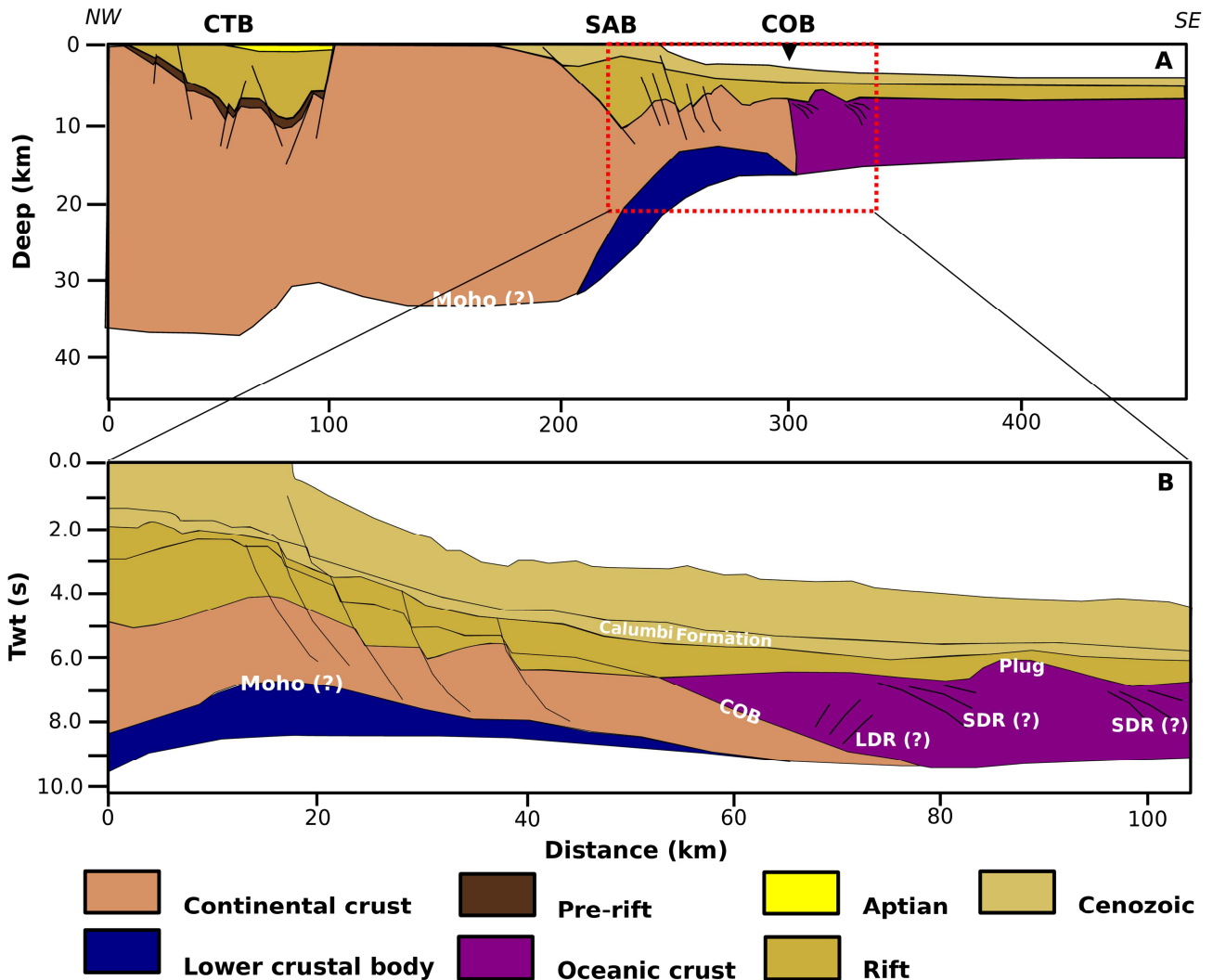


173 *Figure 3: a) Gravity modelled transect in SAB modified from Blaich et al. (2008), represented by the blue line in figure*
174 *1. The red dotted square in the gravity model represents the location of the seismic profile 239-RL-343, the area inside*
175 *the square was modelled based on seismic data and the rest on gravity data; b) Interpreted deep seismic profile 239-*
176 *RL-343 by Mohriak et al. (1995, 1998, 2000), represented by the red line in figure 1. CTB, Central Tucano Basin; SAB,*
177 *Sergipe Alagoas Basin; COB Continental-Oceanic Boundary; SDR, Seaward Dipping Reflectors; LDR, Landward*
178 *Dipping Reflectors.*

179

## Data Processing and Modeling

180
181 The ION-GXT profiles are high quality reflection seismic profiles. However, the time-to-depth
182 inversion made to transform the time data into depth data are not based on high-accuracy crustal P-
183 wave velocities. The SALSA refraction seismic profiles were located following some ION-GXT
184 profiles positions, allowing in the future an integration of more detailed crustal P-wave velocities

7

185   obtained by wide-angle refraction data. During the SALSA experiment, Multi-Channel Seismic

186   (MCS) acquired jointly with refraction data was processed using the Geocluster (CGG Veritas)

187   software. The processing sequence was composed of geometry, wave-equation multiple attenuation,

188   shot-gather predictive deconvolution, time variant band-pass filter, random multiple attenuation,

189   normal move-out, CMP stack and post-stack FK time migration. A last step of seismic data

190   processing is the pre-stack depth migration of the MCS data using the results of wide-angle seismic

191   data modeling, followed by residual move-out analysis. This procedure uses both near-vertical and

192   wide-angle seismic data sets to produce a depth seismic section, which images both the sedimentary

193   crust as well as the basement. Furthermore, it allows to verify the accuracy of the wide-angle

194   velocity model in the sedimentary sequences.

195

196   **Results**

197   Despite the profiles SL01 and SL02 being parallel, 75 km apart, and in the same sedimentary basin,

198   each multi-channel seismic image shows a very different sedimentary stratigraphy and basement

199   geometry (Figure 4). While the southern SL01 MCS record-section shows some chaotic patterns,

200   with heterogeneous layers, sometimes truncations, and a basement with a quite irregular

201   topography, the SL02 MCS record-section, shows some plan-parallel layers (except the seafloor,

202   that is quite irregular in the proximal part). Sometimes, there are some completely seismically

203   transparent areas, which might be associated with erosional boundaries (Figure 4).

204   **SL01**

205   The SL01 line is a 210 km long and NW-SE oriented profile that spans from the continental slope to

206   the distal basin. It is coincident with the ION-GXT 2275 profile and parallel to the associated SL02

207   profile; both refraction profiles were planned to study the crustal architecture of the SAB (Figure 1).

208   At sea, a total of 16 OBS (instruments with four components: Hydrophone plus 3-Comp.

209   Seismometer) were deployed, spaced every 13 km, at water depths of 1 560 m to 4 320 m. The 1376

210   air-gun shots in SL01 were recorded by all instruments. The quality of the recorded signal is very

211   good. This profile crosses two margin parallel profiles designed to image the segmentation (Evain

212   *et al.*, in prep.): the SL06 profile at the SL01OBS02 and the SL05 profile at the SL01OBS03 in the

213   proximal part.

214   In the OBS data, several near-offset reflected and associated refracted arrivals are visible,

215   decreasing in number as we move towards the distal basin.

8

216 From SL01OBS01 onward, the full subsurface sedimentary, crustal, and mantellic sequence is
217 imaged from shots at the vertical of each OBS to offsets reaching 110 km. In addition to clear Pg1,
218 Pg2, Pg3, Pu, Pn (mostly) first arrivals (represented with blue, violet and magenta shades), Ps1 to
219 Ps6 sedimentary refracted arrivals, traveling with apparent velocity increasing from less than 2 km/s
220 (close to the water-cone) up to 3 km/s, are observed as secondary arrivals (represented with red,
221 orange, yellow, and light-green shades). The shallowest layer, is very slow (1.85 km/s) and not very
222 well marked on the seismic profile, but is necessary to fit correctly the secondary later arrivals.
223 From the second to fifth layer, the velocity increases from 2.00 km/s to 3.10 km/s. From
224 SL01OBS01 to SL01OBS03, these layers do not show evidence of clear refracted arrivals and were
225 positioned according to the reflected arrivals. The Ps6 refraction shows top and bottom velocities
226 from 3.35 km/s to 3.45 km/s. Furthermore, at near-critical incidence, high-amplitude reflections are
227 observed, particularly from the tops of the lower crust Pg3P, Unknown unit PuP, and Moho PmP on
228 the seaward-side of OBSs. The Pg1 phase presents the shortest offset span (from ~7.5 to 20 km
229 offset, as we can see in the SL01OBS03 (Figure 5); and the largest curvature indicative of larger
230 velocity gradient. The Pg2 extends from 20 to ~50 km offset and Pg3 from 50 to ~80 km offset and
231 present the lowest apparent velocity gradient.

232 In the distal oceanic part, from 90 to 220 km model distance, from SL01OBS08 (Figure 6) to
233 SL01OBS15 (Figure 7), the data shows only four sedimentary layers and the related phases, Ps1 to
234 Ps4 remain weak, and almost indistinguishable refracted arrival phases that are recorded as a fan of
235 second arrival phases with slightly increasing velocities and relatively low velocity-gradients that
236 emerges from the water cone. These phases were also modelled according to the reflected arrivals..
237 In the presumed oceanic basin, the Pg1, Pg2 and Pg3 refracted phases form a relatively continuous
238 event in both amplitude and apparent velocity, without sharp inflections indicative of major velocity
239 changes between layers. The PuP phase spans from 0 to 80 km model distance with apparent
240 velocity close to Pg3 in the necking zone. Pn is observed emerging at ~70 km offset with an
241 apparent velocity increasing from 7.90 to more than 8.10 km/s and large amplitude variations both
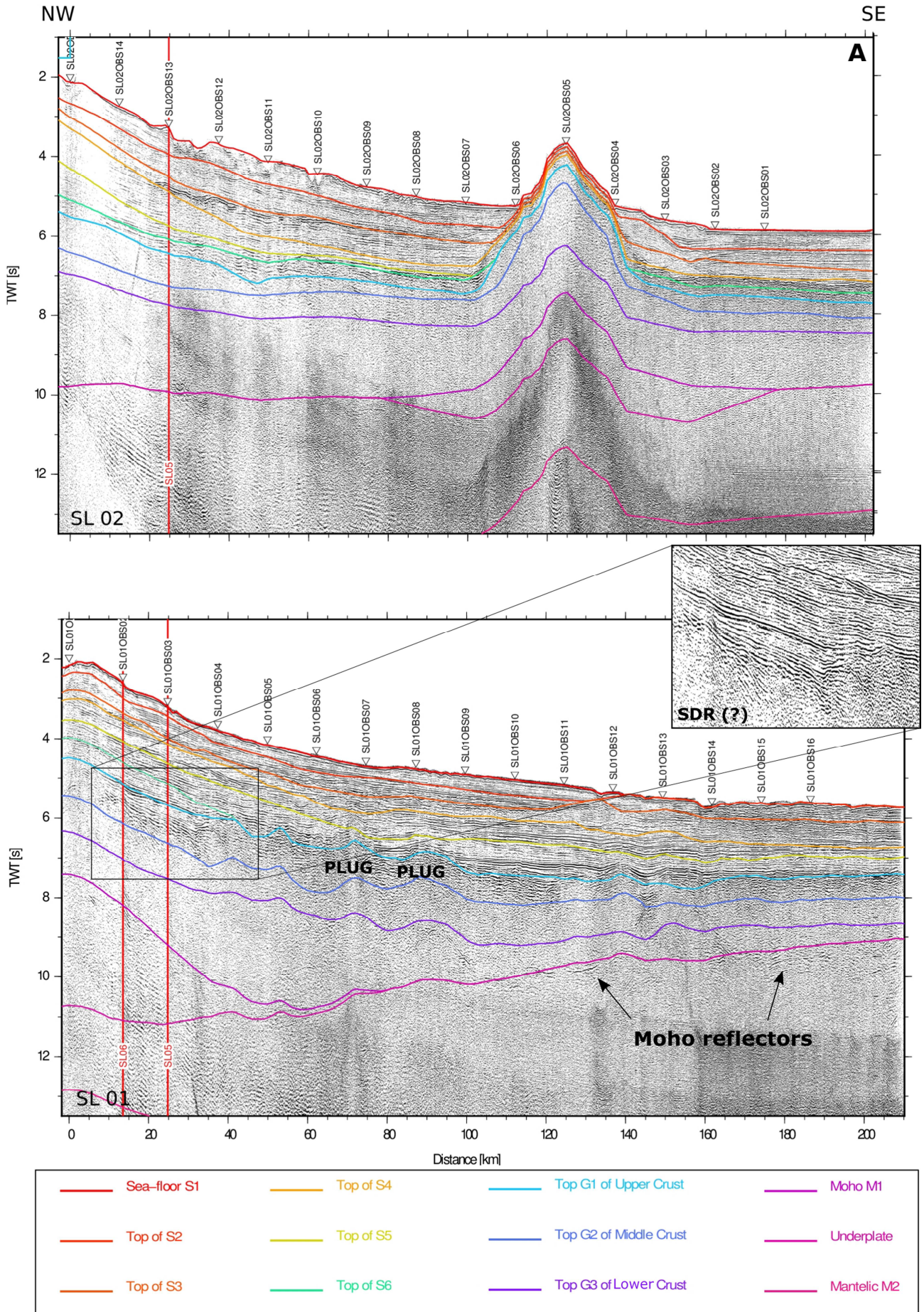242 along offset and OBSs.

243

244

245

246

247

NW

SE

A

SL 02

SDR (?)

PLUG    PLUG

Moho reflectors

SL 01

| Sea–floor S1 | Top of S4 | Top G1 of Upper Crust | Moho M1 |
| Top of S2 | Top of S5 | Top G2 of Middle Crust | Underplate |
| Top of S3 | Top of S6 | Top G3 of Lower Crust | Mantelic M2 |

*Figure 4: Two-way travel-time record section of MCS data along SL02 (A) and SL01 (B) profiles overlain by time converted interfaces of wide-angle model. The intersections with the SALSA dataset are indicated by red line. OBS locations are indicated by white triangle. Vertical exaggeration at seafloor is 1 :12.5*
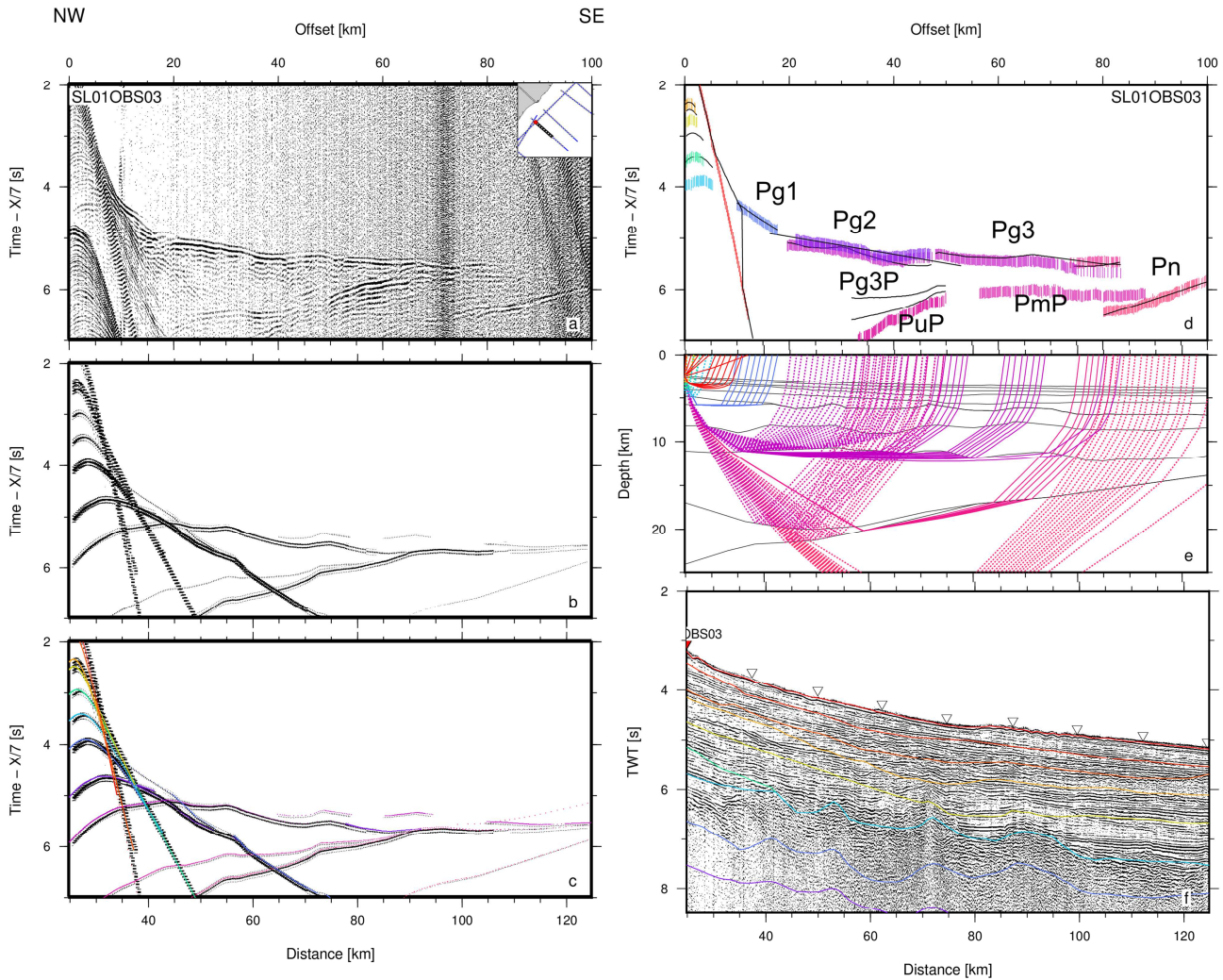


*Figure 5: SL01OBS03 on profile SL01 on the SAB. a) Seismic record; b) Synthetics; c) Color coded synthetic; d) Color coded observed travel-times overlain by predicted times in black; e) Seismic rays; f) MCS time migrated section and color-coded model interfaces. On a, b, c, and d, travel-time is reduced by a velocity of 7 km/s.*

## Velocity model

From SL01 wide-angle data, we digitized 25741 events and interpreted their respective phases. Travel-time uncertainty was estimated on the SL01OBS records and fixed at 0.030 s for the water, 0.050 s for the sedimentary arrivals increasing to 0.100 s for the crustal and mantellic arrivals. The model explains the travel-time and phase of 21204 events or 82% of total picks, with a global RMS travel-time residual of 0.119 s. Given our events individual uncertainty, the model results in a normalized chi-squared of 1.406. Generally, the SL01 model correctly explained the SL01OBS with chi-squared and rms acceptable values (Table 1).

The final velocity model of profile SL01 images all the sedimentary and basement layers to a depth of around 25 km (Figure 8B).

11

265 The model has a sedimentary cover with 6 sedimentary layers in the continental part and 4 layers in
266 the presumed oceanic basin, that reach a thickness of 5 km for all along the profile. S1 has no lateral
267 velocity gradient with top and bottom seismic velocities of 1.75 km/s to 1.80 km/s. S2 has a lateral
268 gradient in the velocities that goes from 2.00 km/s in the western part of the profile and gradually
269 decreases up to 1.80 km/s. The two first sedimentary layers pinch out at 130 km in the distal basin.

270

271

272

273

274

275

276

277

278

279

280

281

| phase | npts | Trms (s) | chi-squared | Uncertainty (ms) |
|---|---|---|---|---|
| water | 2112 | 0.028 | 0.080 | 30 |
| Ps1P | 264 | 0.091 | 0.827 | 50 |
| Ps2P | 10 | 0.076 | 0.641 | 50 |
| Ps3P | 527 | 0.087 | 0.751 | 50 |
| Ps4P | 672 | 0.186 | 3.463 | 50 |
| Ps5P | 243 | 0.097 | 0.943 | 50 |
| Ps6P | 682 | 0.252 | 6.379 | 50 |
| Pg13 | 810 | 0.106 | 1.122 | 100 |
| Pg1P3 | 1582 | 0.104 | 1.081 | 100 |
| Pg23 | 1507 | 0.100 | 1.008 | 100 |
| Pg33 | 2173 | 0.100 | 1.004 | 100 |
| Pg3P3 | 4916 | 0.127 | 1.605 | 100 |
| Pn3 | 3048 | 0.113 | 1.274 | 100 |
| PmP3 | 535 | 0.204 | 4.163 | 100 |
| Pu3 | 419 | 0.222 | 4.924 | 100 |
| Pup4 | 1483 | 0.242 | 5.859 | 100 |

282 *Table 1: Reflected or refracted phase name, number of explained events, residual mean-square, and normalized chi-*
283 *squared value for the SL01 model.*

284 S3 has top and bottom velocities from 2.40 km/s to 2.50 km/s. S4 has regular top and bottom
285 velocities from 2.85 km/s to 3.00 km/s. S5 has also regular top and bottom velocities from 3.10
286 km/s to 3.15 km/s on the distal basin and a constant velocity of 2.95 km/s on the continental slope.
287 S6 appears only in the continental slope zone, over a basement depression, and pinches out at 40 km
288 and has top and bottom velocities from 3.35 km/s to 3.45 km/s.

289 The lithospheric structure has five layers: upper crust, middle crust, lower crust, anomalous velocity
290 zone and lithospheric mantle. The upper crust has a thickness of 2.5 km on the continental slope and
291 decreases to 1.0 km and 1.5 km on the distal basin with a very irregular topography, full of basins
292 and mounts, with velocities at the top and bottom of 5.00 km/s and 5.10 km/s, a little decrease to
293 4.85 km/s at 110 km and increases to 5.10 km/s and 5.20 km/s at the distal basin. The middle crust
294 has regular thickness of 2.5 km for all along the profile, with velocities at the top and bottom from
295 6.50 km/s to 6.60 km/s. The lower crust starts with a thickness of 5 km in the very northwestern

296 part of the profile, and thickens to 10 km between 20 and 70 km and thins to 3.0 km towards the

297 ocean, with velocities at the top and bottom from 7.00 km/s to 7.20 km/s.
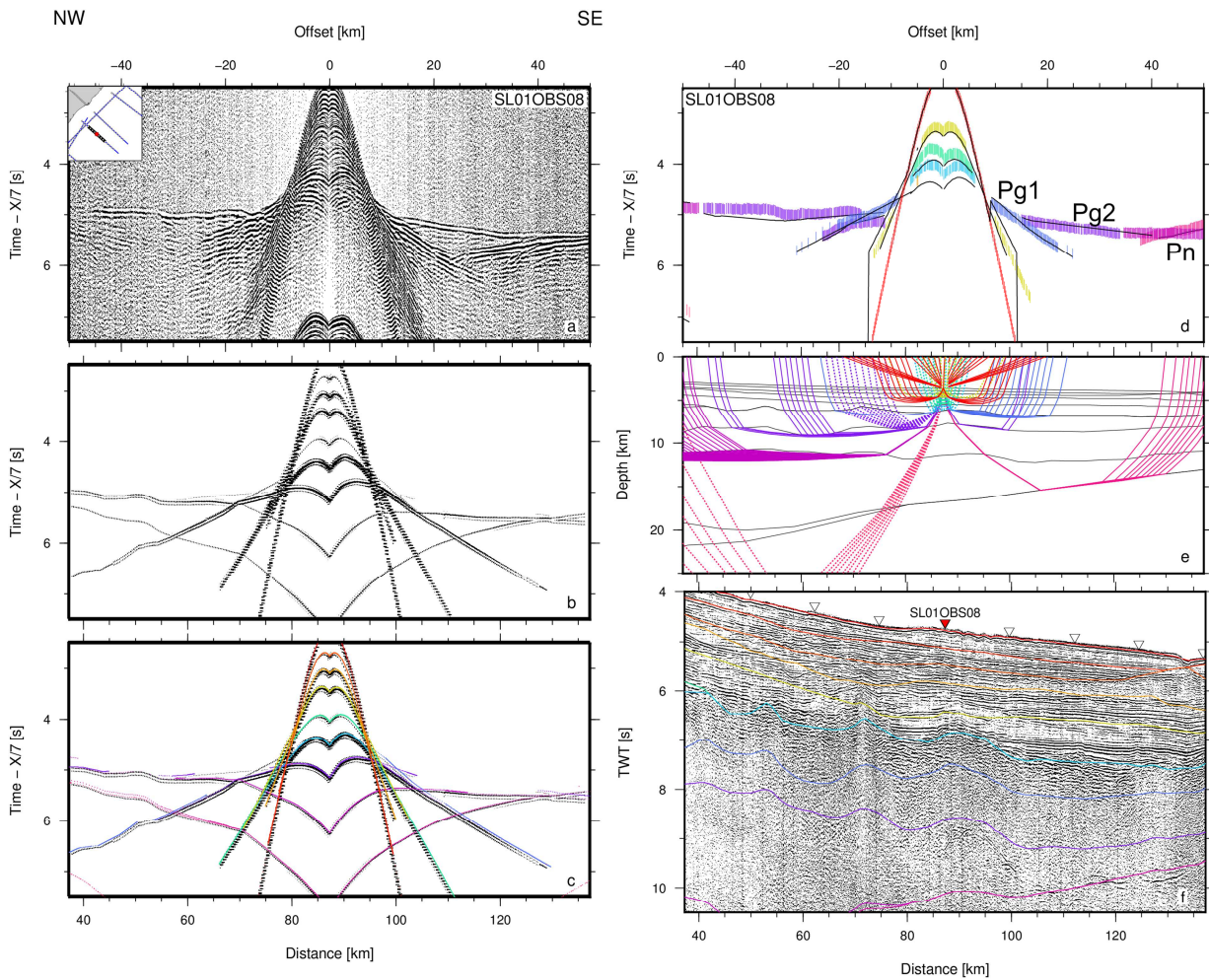


298 *Figure 6: SL01OBS08 on profile SL01 on the SAB. a) Seismic record; b) Synthetics; c) Color coded synthetic; d) Color*

299 *coded observed travel-times overlain by predicted times in black; e) Seismic rays; f) MCS time migrated section and*

300 *color-coded model interfaces. On a, b, c, and d, travel-time is reduced by a velocity of 7 km/s.*
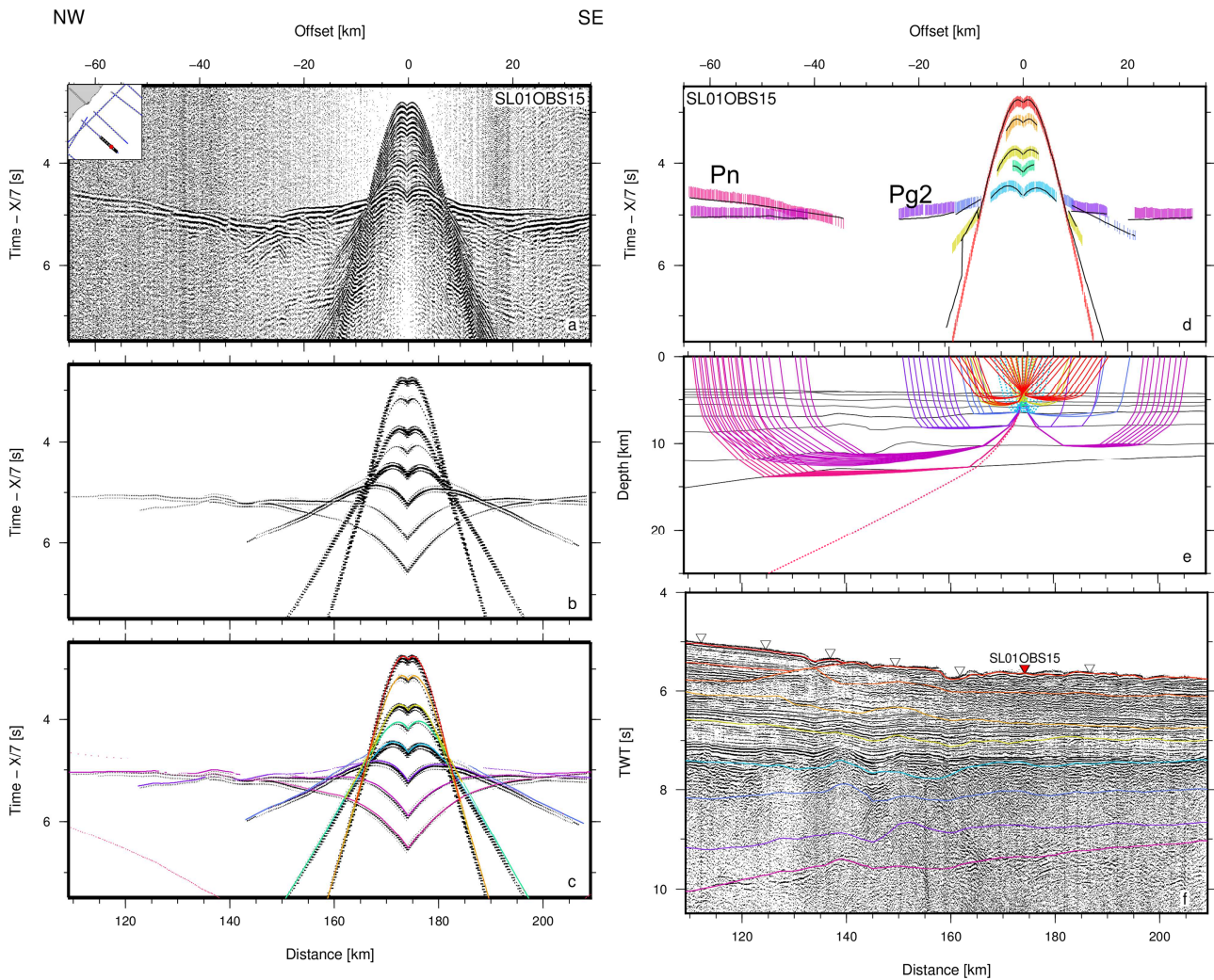
301

302

303

304

305

306

307

308

309

310

311



312

*Figure 7: SL01OBS15 on profile SL01 on the SAB. a) Seismic record; b) Synthetics; c) Color coded synthetics; d) Color-coded observed synthetic; d) Color coded observed travel-times overlain by predicted times in black; e) Seismic rays; f) MCS time migrated section and color-coded model interfaces. On a, b, c, and d, travel-time is reduced by a velocity of 7 km/s.*

The anomalous velocity zone, located at the necking zone, is badly constrained, showing its possible reflected arrival only in the two most proximal OBSs. These reflected arrivals can also be the result of an internal reflector, representing some intra-crustal body. With this information and the ION-GXT data (Figure 8B), this zone was modeled with 10 km thickness, that thins abruptly until pinching out against the lower crust at 80 km. This zone presents velocities between the top and the bottom from 7.20 km/s to 7.25 km/s. The top of the lithospheric mantle below the Moho has a velocity of 7.90 km/s. Note that an additional lithospheric layer located at 10 to 15 km below the Moho, with 8.10 km/s, is necessary to provide a gradient capable of explaining the Pn arrivals. It is

14

325 well constrained in the proximal part of the two profiles, but only in the distal part of SL02 profile
326 (Figure 8A).

327

328 **SL02**

329 The SL02 line is a 220 km long and NW-SE oriented profile, parallel to SL01, that spans offshore
330 from the continental platform to the distal basin. The SL02 was extended inland along a distance of
331 150 km from the most proximal OBS, for a total profile length of 370 km. It is coincident with the
332 ION-GXT 2300 profile (Figure 8A).

333 At sea, a total of 15 OBS (instruments with four components: Hydrophone plus 3-Comp.
334 Seismometer) were deployed, spaced every 13 km, at water depths of 1.557 to 4.368 m (Figure 1C).
335 The 1271 air-gun shots in SL02 were recorded by all instruments. The quality of the recorded signal
336 is very good. Inland, the profile was extended 150 km towards the North-West with the deployment
337 of 21 Land Seismic Stations (LSS, spaced every 5 km). The profile has 100 km of extension
338 because, unfortunately, there is a gap of about 50 km between the last LSS and the first OBS, on the
339 inner shelf. This profile crosses the SL05 profile at the position of the SL02OBS02 and
340 SL05OBS14, in proximal position.

341 The geometry of the sedimentary and crustal layers onland beneath the seismic land stations can
342 further be constrained from geological and geophysical studies conducted in the study area (Chang
343 *et al.,* 1992; Soares *et al.,* 2010; Tavares *et al.,* 2012; de Lima *et al.,* 2015). Surface geology
344 indicates the Sergipano Fold Belt from SL02LSS11 to SL02LSS01, and an outcrop of Quaternary
345 deposits from SL02LSS21 to SL02LSS10, as shown at the SL02LSS15 (Figure 9).

15
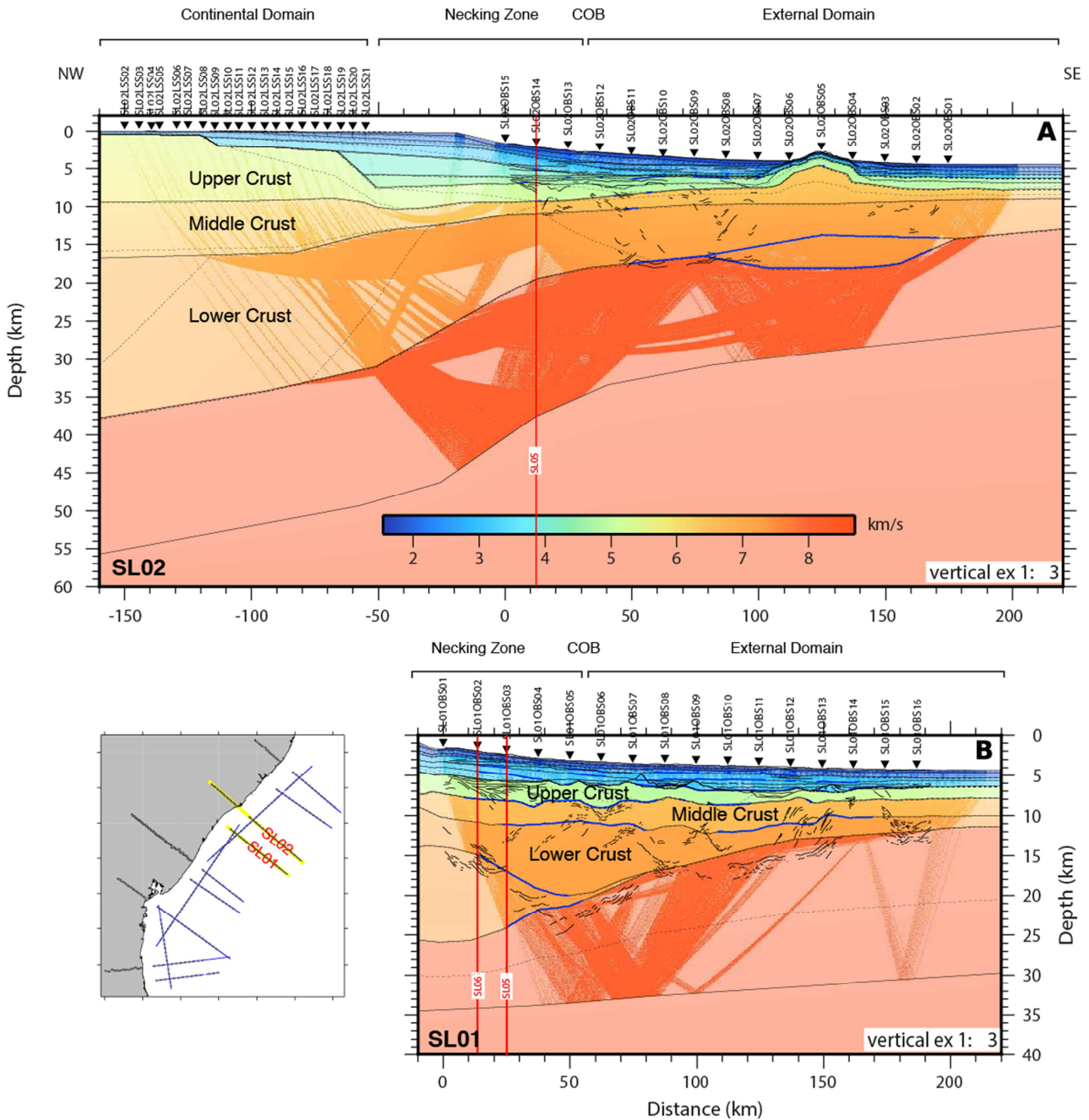
*Figure 8: Final P-wave interval velocity models along SL02 (A) and SL01 (B) profiles overlaid by the respective line-drawing of the ION-GXT lines. Black lines mark model layer boundaries. Colored area is constrained by seismic rays. Inverted black triangle mark OBS and LSS positions. Thick blue lines mark the interfaces where reflections are observed on the wide-angle records. Black dotted lines correspond to isocontours. Vertical red lines indicate crossing profiles. Vertical exaggeration is 1:3.*

Refracted events in the continental crust middle-crust Pg2 in light-blue, lower-crust Pg3 in blue and Pn in violet are relatively strong and allow to constrain the crustal structure from –160 to 0 km model-distance (Figure 9). Pn arrivals refracted from as deep as 30 km beneath the un-thinned

356 continental margin traveling at 8 km/s apparent velocity. PmP arrivals from 150-160 km offset

357 reflect from the hinge-line where the continental crust begins to thin.
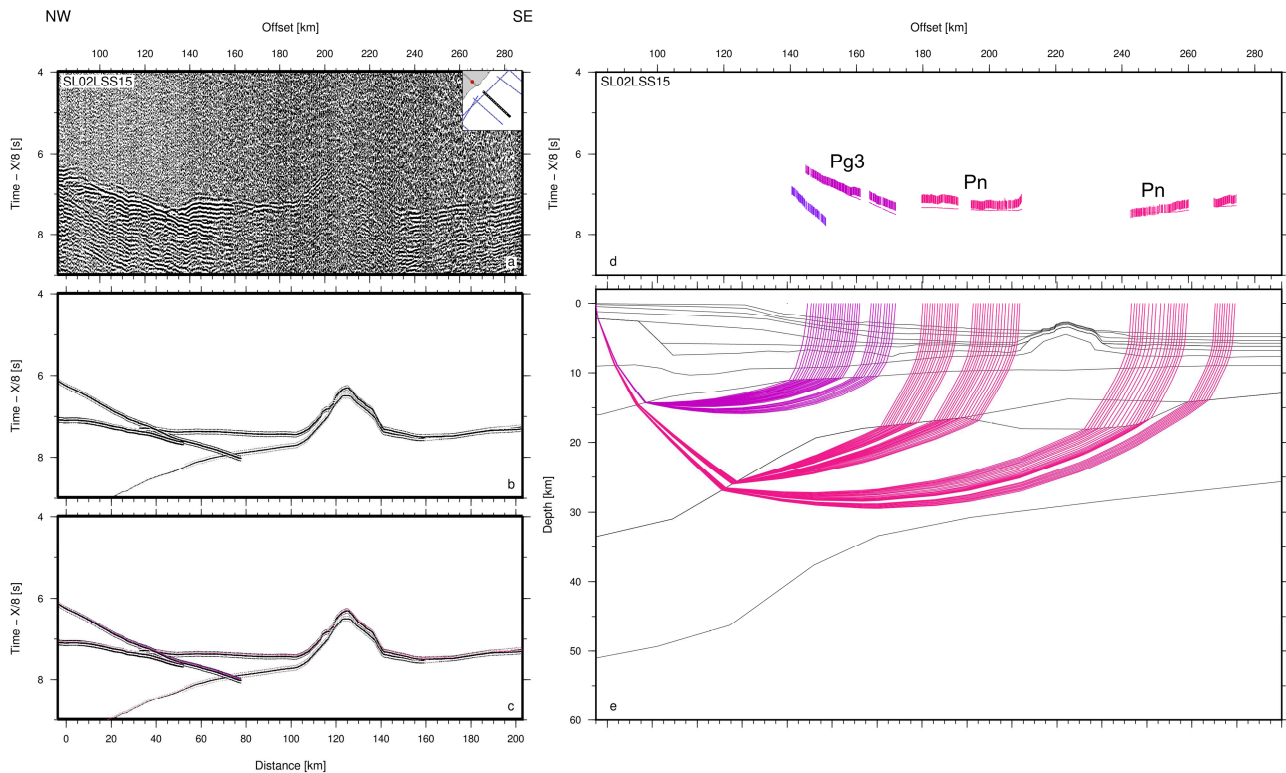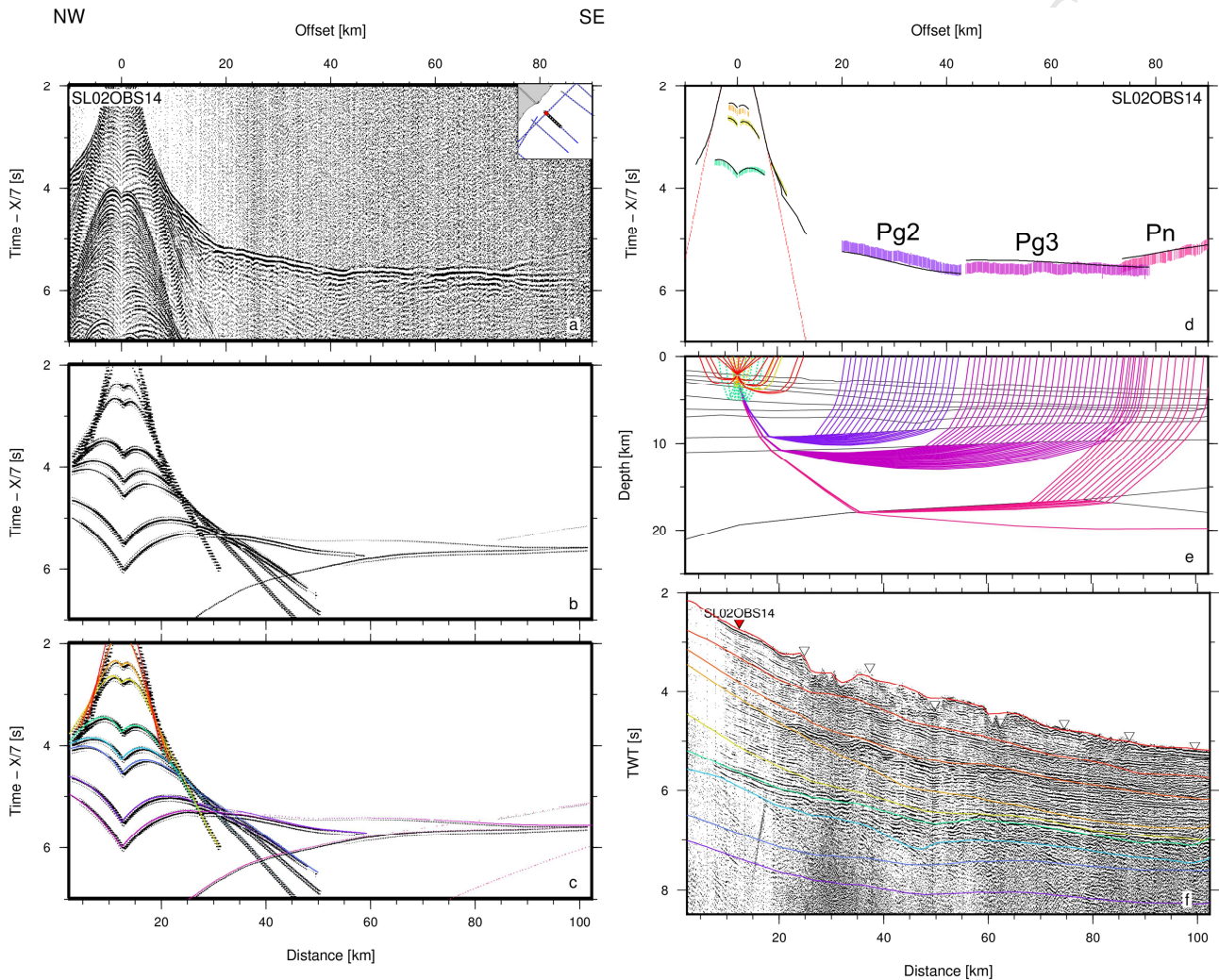


358 *Figure 9: SL02LSS15 on profile SL02 on the SFB/SAB contact. a) Seismic record; b) Synthetics; c) Color coded*

359 *synthetic; d) Color coded observed travel-times overlain by predicted times in black; e) Seismic rays. On a, b, c, and d,*

360 *travel-time is reduced by a velocity of 8 km/s.*

361

362 From SL02OBS15 onward, the full subsurface sedimentary, crustal and mantellic sequence is

363 imaged from shots at the vertical of each OBS to offsets reaching 110 km. The SL02OBS14 (Figure

364 10) shows the example of this part. In addition to clear Pg1, Pg2, Pg3, Pu, Pn (mostly) first arrivals

365 (represented with blue, violet and magenta shades), Ps1 to Ps6 sedimentary refracted arrivals,

366 traveling with apparent velocity increasing from less than 2 km/s (close to the water-cone) up to 4

367 km/s, are observed as secondary arrivals (represented with red, orange, yellow, and light-green

368 shades). At ~60 km distance, the Ps5 disappears, and the profile continues seawards with only 5

369 sedimentary layers. Furthermore, at near-critical incidence, high-amplitude reflections are observed,

370 particularly from the tops of the lower crust Pg3P, unknown unit PuP, and Moho PmP on the

371 seaward-side of OBSs. The Pg1 phase presents the shortest offset range (from ~7.5 to 20 km offset),

372 and the largest curvature indicative of large velocity gradient. The Pg2 extends from 20 to ~40 km

373 offset and Pg3 from 45 to ~80 km offset and the lowest apparent velocity gradient.

374 In the distal part, from 90 to 140 km model distance, as shown in SL02OBS07 (Figure 11), the Ps1

375 to Ps4 remain weak and almost undistinguishable refracted arrival phases that are recorded as a fan

376 of second arrivals with slightly increasing velocities and relatively low velocity-gradients that

17

emerges from the water cone. The Ps5 refraction shows considerably higher amplitude and apparent

velocity: the exact nature of the S6 layer represented by this phase must be further examined from

the pre-stack depth migration of the MCS data, for instance. In the distal oceanic part, the Pg1, Pg2

and Pg3 refracted phases form a relatively continuous event in both amplitude and apparent

velocity, without sharp inflections indicative of major velocity changes between layers. The Pu

phase spans from 90 to 140 km offset and has an apparent velocity close to Pg3. Pn is observed



emerging at ~75 km with an apparent velocity increasing from 7.9 to more than 8.15 km/s and large

amplitude variations both along offset and OBSs.

*Figure 10: SL02OBS14 on profile SL02 on the SAB. a) Seismic record; b) Synthetics; c) Color coded synthetic; d)*
*Color coded observed travel-times overlain by predicted times in black; e) Seismic rays; f) MCS time migrated section*
*and color-coded model interfaces. On a, b, c, and d, travel-time is reduced by a velocity of 7 km/s.*

### Velocity Model

From SL02 wide-angle data, we digitized 24009 events and interpreted their respective phases.

Travel-time uncertainty was estimated on the SL02OBS and SL2LSS records and fixed at 0.030 s

for the water, 0.050 s for the sedimentary arrivals increasing to 0.100 s for the crustal and mantellic

18

arrivals. The model explains the travel-time and phase of 21166 events or 88% of total picks, with a global RMS travel-time residual of 0.138 s. Given our events individual uncertainty, the model results in a normalized chi-squared of 1.892. Generally, the SL02 model correctly explained the SL02OBS and SL02LSS with chi-squared and rms values acceptable (Table 2).

| phase | npts | Trms | chi-squared | Uncertainty (ms) |
|---|---|---|---|---|
| water | 2708 | 0.029 | 0.084 | 30 |
| Ps1P | 21 | 0.013 | 0.017 | 50 |
| Ps2P | 436 | 0.070 | 0.496 | 50 |
| Ps3P | 305 | 0.085 | 0.727 | 50 |
| Ps4P | 298 | 0.067 | 0.444 | 50 |
| Ps5P | 122 | 0.154 | 2.394 | 50 |
| Ps6P | 277 | 0.102 | 1.042 | 50 |
| Pg1 | 43 | 0.113 | 1.308 | 100 |
| Pg1P | 32 | 0.186 | 3.570 | 100 |
| Pg2 | 347 | 0.167 | 2.793 | 100 |
| Pg2P | 30 | 0.052 | 0.282 | 100 |
| Pg3 | 1893 | 0.131 | 1.706 | 100 |
| Pg3P | 1980 | 0.121 | 1.470 | 100 |
| Pn | 7194 | 0.121 | 1.462 | 100 |
| PmP | 1083 | 0.145 | 2.101 | 100 |
| Pu | 38 | 0.052 | 0.274 | 100 |
| PuP | 1078 | 0.243 | 5.906 | 100 |

*Table 2: Reflected or refracted phase name, number of explained events, residual mean-square, and normalized chi-squared value.*

The final velocity model of profile SL02 images the depth geometry of all sedimentary, crustal and mantellic layers to a depth of around 34 km (Figure 8A). According to the interpretation of the wide-angle data described above the velocity structure of SL02 model was modeled using four to six layers of sediments. These sedimentary layers are characterized by relatively homogeneous P-wave velocities all along the SL02 model with no strong lateral variation. This sedimentary deposit in the SAB starts at –120 km model distance and reaches a maximum of 7 km of thickness between -50 and -20 km model distance until 2.5 km at the SE in the distal basin (Figure 8A).

407
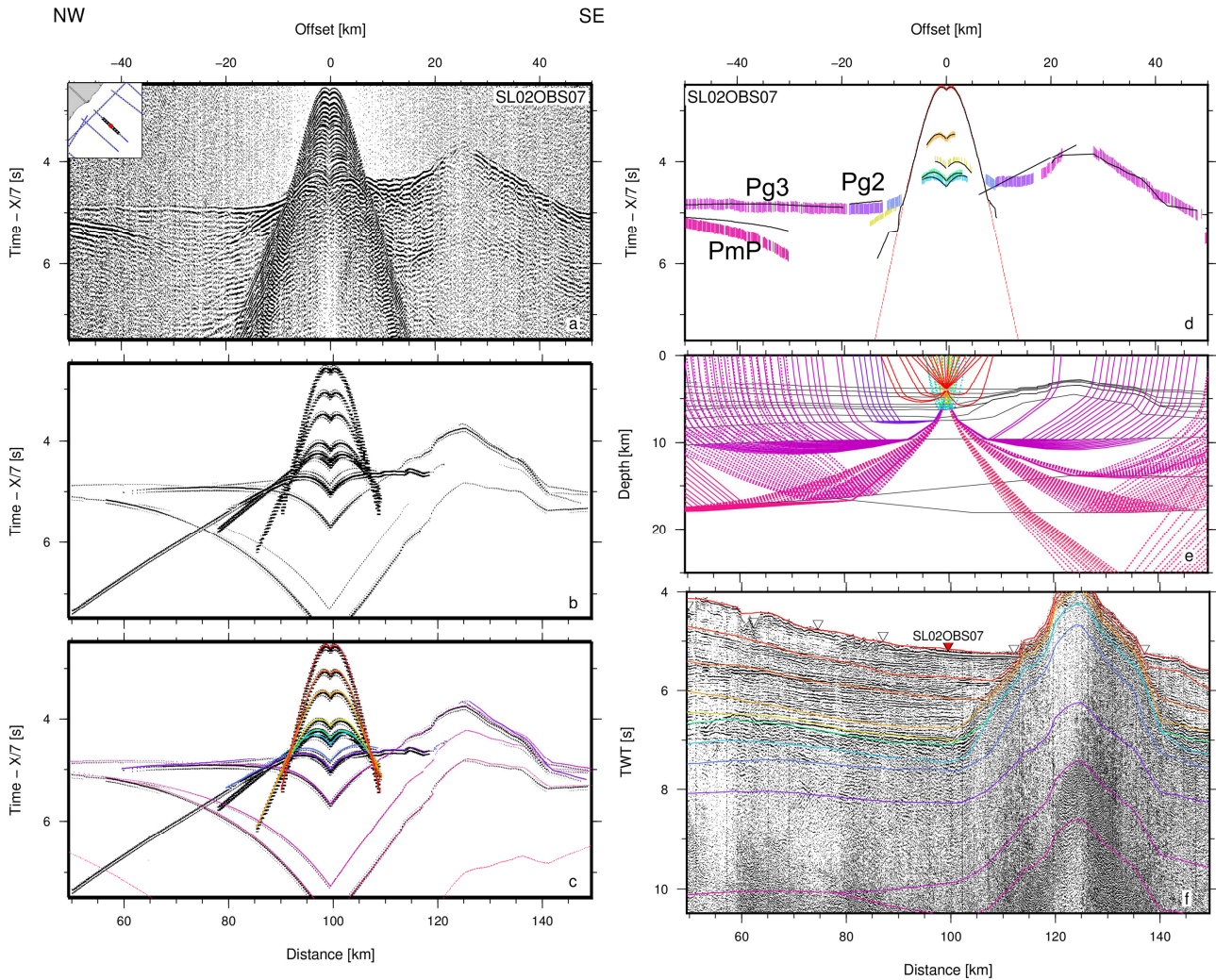
*Figure 11: SL02OBS07 on profile SL02 on the SAB. a) Seismic record; b) Synthetic; c) Color coded synthetic; d) Color coded observed travel-times overlain by predicted times in black; e) Seismic rays; f) MCS time migrated section and color-coded model interfaces. On a, b, c, and d, travel-time is reduced by a velocity of 7 km/s.*

411

The P-wave velocities of the sedimentary sequence show an increasing trend: the top velocity at the seafloor is 1.65 km/s (S1) and the maximum velocity 4.7 km/s is reached at the base of the sedimentary sequence (S6).

S1 has top and bottom P wave seismic propagation velocities of 1.65 km/s to 1.85 km/s. S2 has a negligible vertical gradient and propagation velocity of 2.2 km/s on the western end of the profile that gradually decreases up to 2.10 km/s. S3 has top and bottom velocities from 2.60 km/s to 2.70 km/s with a small gradient decrease towards the continental slope. S4 has top and bottom velocities from 3.00 km/s to 3.25 km/s. S5 has top and bottom velocities from 4.10 km/s to 4.20 km/s. S6 has constant top and bottom velocities from 4.60 km/s to 4.70 km/s.

421 Beneath this sedimentary record, the top of the basement corresponds to a rough interface and the

422 modeled basement structure comprises four crustal layers: upper crust, middle crust, lower crust and

423 an anomalous body under the volcano. The upper crust has a thickness between 1.0 km and 2.0 km

424 on the presumed oceanic basin and increases to 3.0 km at the continental slope, with velocities at

425 the top and bottom from 4.75 km/s to 5.1 km/s.

426 The middle crust has a regular thickness of 3.0 km for all the profile, except under the volcano,

427 where it reaches almost 5.0 km with velocities at the top and bottom from 6.4 km/s to 6.5 km/s on

428 the continental slope and from 6.2 km/s to 6.3 km/s on the distal basin. The lower crust is 8.0 km

429 thick at the northwestern end of the model and completely thins out to 4.0 km thick towards the

430 ocean, with velocities at the top and bottom from 6.90 to 7.10 km/s along all the profile, except in

431 the necking zone, between 0 and 50 km model distance, where there is a slight increase of the

432 velocities in the middle and the lower crusts: the middle crust passes from 6.10-6.30 km/s to 6.30-

433 6.50 km/s and the lower crust, from 6.90-7.10 km/s to 7.30-7.50 km/s (Figure 8B). Note that there

434 is also a thick anomalous body, not located below the Necking Zone as along SL01 profile, but

435 below the Moho in the volcanic edifice area. It has a thickness of 8 km and velocities between 7.3-

436 7.4 km/s.

437 ## Evaluation of the models

438 **Gravity modelling**

439 A 2-D model consisting of homogeneous density blocks was constructed from the seismic velocity

440 model: the P-wave velocity is converted to densities according to Ludwig *et al.* (1970) except

441 onshore in the continental crust where conversion follows Christensen and Mooney (1995). The

442 resulting density ranges from 2200 to 2500 kg/m³ in the basin, 2600 to 2750 kg/m³ in the crust and

443 3000 to 3170 kg/m³ in the under-crustal unit. The mantle density is set at 3420 kg/m³. The model is

444 extended down to 80 km where isostatic compensation may be reached, and the modeled free-air

445 anomaly is compared to measured gravity anomaly along the SL01 and SL02 profiles (Figure 12).

446 The SL01 model fits relatively well (within less than 10 mGal) the gravity data acquired offshore

447 during the SALSA survey, except for the continental slope (where the model is less constrained)

448 where there's a misfit of 17 mGal. Free air gravity from satellite data (Sandwell *et al.*, 2014)

449 extracted along the profile and 10, 20, and 30 km cross-line presents broad (>50 km wavelength)

450 along profile and lateral scatter amplitude variations of +/- 10 mGal (Figure 12c and d).

451 The SL02 model fits relatively well (within less than 25 mGal) the gravity data acquired offshore

452 during the SALSA survey, except for the seamount where there's a misfit of 65 mGal, probably due

453 to the 3D effects. The calculated gravity anomaly falls well within the values observed on parallel

21

454  profiles extracted north and south of the profile (Figure 12a and b), derived from satellite gravity

455  measurements (Sandwell *et al.*, 2014). Due to the high altitude of the satellite, lower wave-length

456  are not well recorded.

457



458
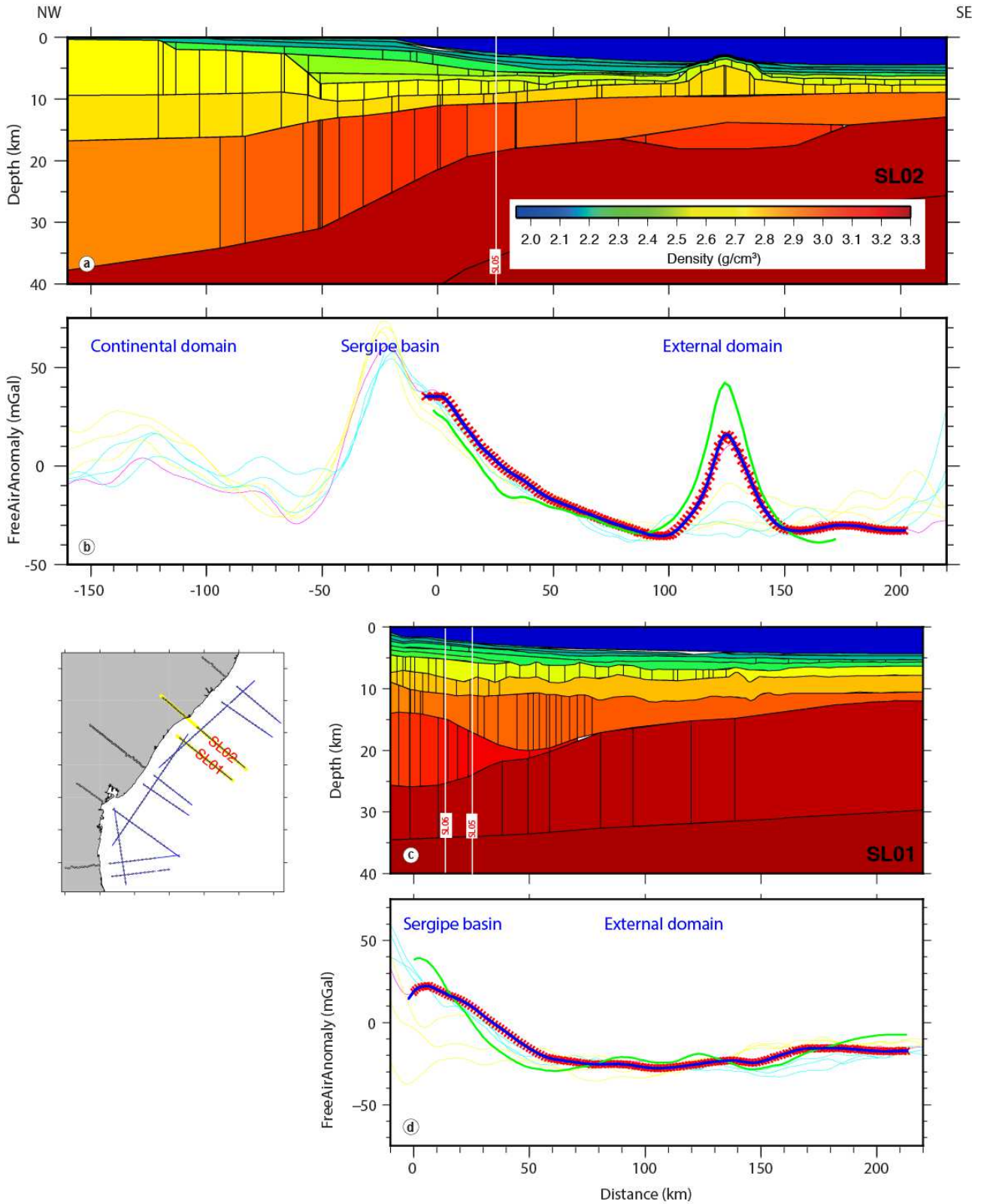
*Figure 12: Gravity modeling along SL02 profile. a) Density model up to a depth of 40 km overlain by interfaces from wide-angle modeling. b) Free-air gravity anomaly observed (Pavlis et al., 2012 for the offshore data and BGI: International Gravimetric Bureau, for the land data) along the SL02 profile (red crosses) and laterally 10, 20 and 30 km (SW-ward as yellow lines, NE-ward as cyan lines), measured during the SALSA experiment (blue line) and calculated (green line). Gravity modeling along SL01 profile. c) Density model up to a depth of 40 km overlain by interfaces from wide-angle modeling. d) Free-air gravity anomaly observed (Pavlis et al., 2012) along the SL01 profile (red crosses) and laterally 10, 20 and 30 km (SW-ward as yellow lines, NE-ward as cyan lines), measured during the SALSA experiment (blue line) and calculated (green line).*

## Hitcount, spread, and resolution

Interface depth node spacing as well as velocity node spacing is key to model the lateral variations of the seismic velocity with sufficient resolution, but without introducing spurious and unwarranted complexity. Although all synthetics section correctly reproduces the observed amplitude on the wide-angle data (Figures 5 to 11), suggesting a good parameterization of the model, we perform evaluation tests of the P-wave velocity models: hitcount, Spread Point Function (SPF) and resolution (Figure 13).

The interface nodes are spaced at less than 2 km on the seafloor where depth is well constrained by multi-beam bathymetry. Node spacing increases to 2.5 km for the three first sedimentary layers then 5 km for the deepest sedimentary layers and the basement where the interface geometry is well constrained in twt from the MCS data, then 10 km for the middle crust, 15 km for the lower crust and Moho, 30 km and 50 km for the intra-mantellic reflectors. The velocity nodes are not spaced evenly but located where velocity changes are warrant by the observed wide-angle records, resulting in node spacing ranging from 30 to 350 km. The total standard deviation for depth nodes and velocity nodes is 6.229 km and 1.785 km/s, respectively. Most interface and velocity nodes in our experiment produce a hit-count larger than 3000 rays (Figure 13) with exception of the edges of our survey and the middle crust. The Spread Point Function (Figure 13) is indicative for a given velocity variation of the resulting travel-time variations when taking the different ray paths into account. Depth and velocity node SPF is relatively homogeneous in the models except in the lower crust along SL02 profile in the transition of the continental to the presumed oceanic domain. Finally, the diagonal terms of the resolution matrix are a measurement of the spatial averaging of the true earth structure by a linear combination of model parameters (Zelt 1999). Typically, resolution matrix diagonals greater than 0.5–0.7 are said to indicate reasonably well-resolved model parameters (e.g. Lutter and Nowack 1990). The major part of the interface and velocity nodes present good resolution (>0.7). Resolution is poorest at the transition zone, in the lower crust, in the upper crust at the SAB, and under the volcanic edifice (Figure 13).

494
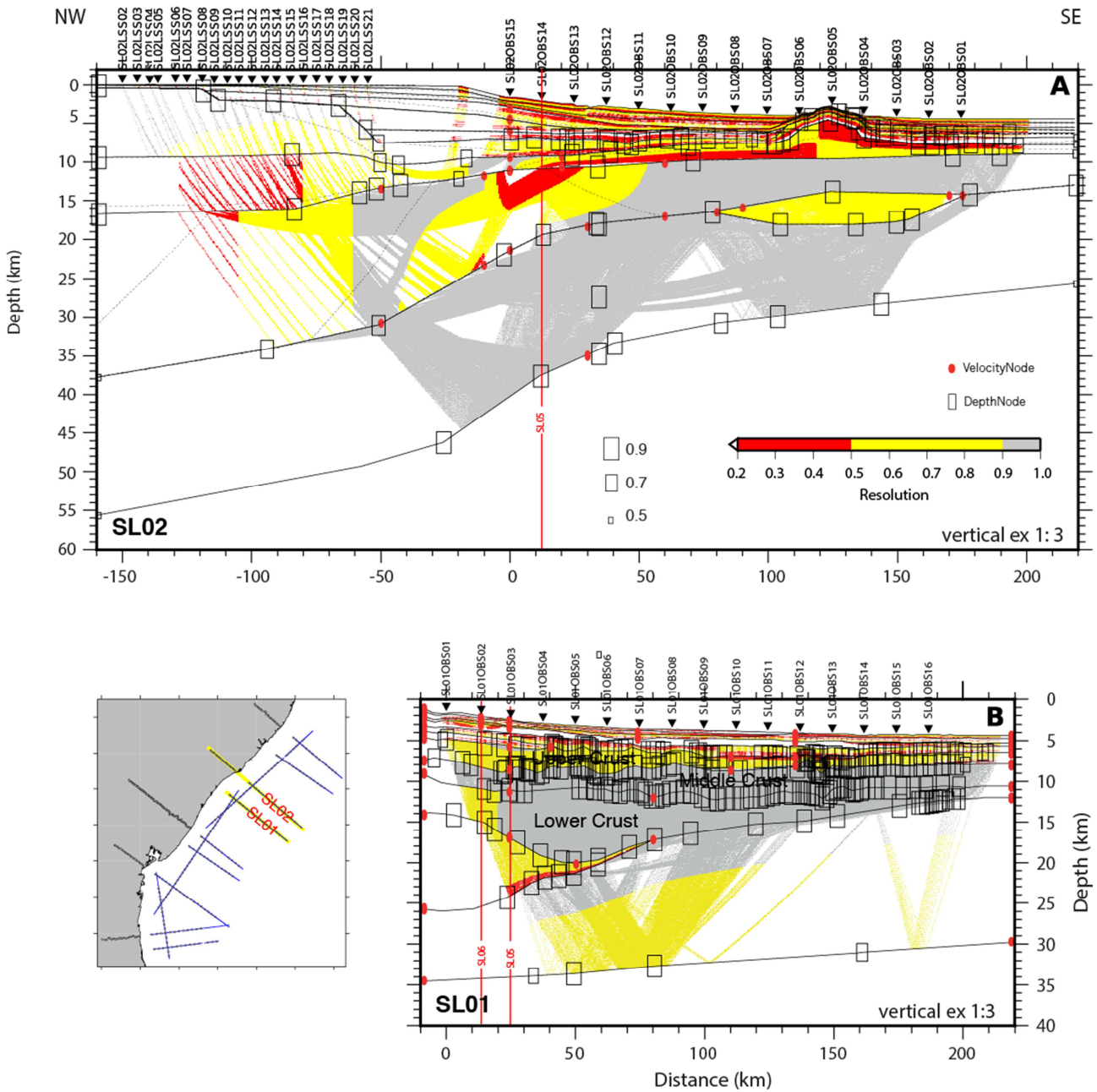
*Figure 13: Evaluation of the wide-angle models SL01 (A) and SL02 (B): Resolution of velocity (gridded and colored). There are zones that were not imaged due to the lack of ray coverage.*

## MCS data pre-stack depth migration (PSDM)

To verify the accuracy of the wide-angle velocity model, the MCS data is pre-stack depth migrated and residual move-out analysis is performed. The pre-processing sequence is identical to the MCS data time processing, and includes geometry, wave-equation multiple attenuation, shot-gather predictive deconvolution, time variant band-pass filter, and random multiple attenuation. The PSDM processing is undertaken using the Seismic Unix package (Stockwell Jr., 1999; Cohen and Stockwell Jr., 2010). The PSDM consists in 2 steps: ray tracing and seismic data depth migration.

24

504  First, the velocity model is utilized to compute travel-time tables regularly spaced at 150 m along

505  the profile by paraxial ray tracing on a $50 \times 25$ m spaced grid, then travel-times in shadow zones are

506  compensated by solving the eikonal equation. Secondly, common offset Kirchhoff depth migration

507  is performed: Migrated traces are output as common image gathers (CIG) binned at 25 m with 30

508  offset-classes between 249 and 4596 m at 150 m spacing. Dip-independent velocity analysis can

509  then be performed on the migrated CIG by analyzing residual move-out. Hence, if the velocity

510  model used for migration is close to the true medium velocity, all common offset migrated panels

511  map the recorded seismic events to the same reflector depth, else the move-out from near to far

512  offset translates into an interval velocity correction (Liu and Bleistein, 1995). Figure 14 presents the

513  PSDM section and CIG gathers extracted every 7.5 km along the two profiles. Moreover, depth

514  migrated gathers are excellent records of amplitude variations with offset (AVO), and therefore are

515  indicators of in-situ rheological changes. The residual move-out behavior together with the seismic

516  character from PSDM images are key elements to locate accurately major geological contacts,

517  moreover with higher horizontal resolution when compared to the OBS records.

518  SALSA01 (Fig. 14C) and SALSA02 (Fig. 14A) were migrated up to a depth of 18 km, showing

519  very good resolution in the sedimentary layers, and a good resolution in the crust, with good

520  agreement between strong reflectors and their wide-angle estimated depths. The SAB shows a

521  sedimentary structuration that can be subdivided between upper and lower packages. Upper

522  sediments represent the first 4 layers, which are finely stratified and made of low amplitude

523  continuous reflectors while deeper reflectors have a stronger amplitude character. The entire

524  sedimentary package is clearly interrupted by the volcanic edifice. The upper package varies in

525  thickness from about 1.5 km at the continental slope, 3 km at NW side of the volcano and 2 km at

526  SE side, at the presumed oceanic basin. The lowest sedimentary package is composed by 2 layers

527  that merge into 1 layer, at 40 km model distance on SL01, and at the NW side of the volcano at

528  SL02. The top of this package shows the strongest and most continuous reflector in the MCS data.

529  This reflector represents the base of the Calumbi Formation.  A recede at the sea level in the end of

530  the Coniacian controlled the erosion of the underlying sequences. This regional erosional event is

531  represented by the so called Pre-Calumbi Formation (probably Santonian, ~86 Ma) unconformity at

532  the base of the Piaçabuçu Group (Mohriak *et al*., 1998; Campos Neto *et al*., 2007). This

533  unconformity can be observed as the most remarkable reflector, and is interpreted as a regional

534  angular, intra-Cretaceous unconformity in the platform that is almost flat-lying in the deep-water

535  region and overlies horizontal sedimentary layers (Mohriak *et al*., 1998, 2000).

536  The basement is composed by chaotic seismic facies in the MCS data. Below the basement it is

537  impossible to differentiate any seismic facies or structure. Unlike the profile SL01 (Figure 4), no

538  reflector corresponding to the Moho is observed in the profile SL02.

539



540
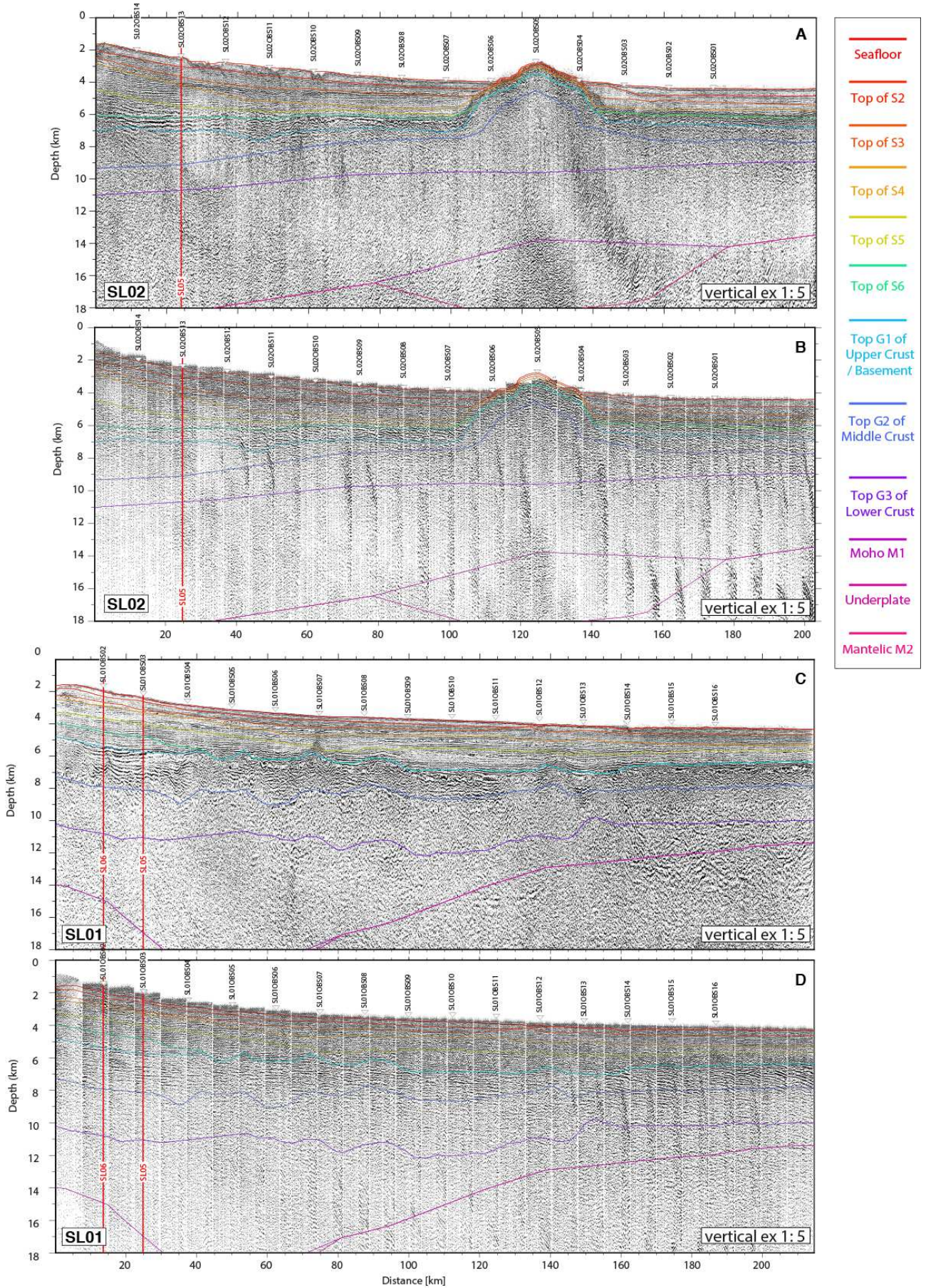
541 *Figure 14: a) Pre-stack depth migrated record section of MCS data along SL02 profile. Model's interfaces are*

542 *represented with continuous lines. The intersections with the SALSA dataset are indicated by red line. Vertical*

26

543 *exaggeration is 1:5. b) Residual move-out of MCS data along SL02 profile. Common image gathers are spaced every*

544 *7.5 km. c) Pre-stack depth migrated record section of MCS data along SL01 profile. Vertical exaggeration is 1:5. b)*

545 *Residual move-out of MCS data along SL01 profile. Common image gathers are spaced every 7.5 km. Vertical*

546 *exaggeration is 1:5.*

547

## Discussion

548 Discussion

549 In order to constrain the nature of the crust, 1D crustal velocity- depth (Vz) profiles were extracted

550 underneath the top of the basement at a 10 km interval from the final velocity models (Figure 15).

551 These Vz graphs can be compared to compilations for typical continental crust (Christensen and

552 Mooney, 1995) and Atlantic-type oceanic crust (White *et al.,* 1992) that allow to discuss the

553 properties of crust and to establish the lateral segmentation along the profiles.

554 On the base of this analysis of the final models and these Vz graphs, three distinct domains can be

555 distinguished: 1. Unthinned Continental Domain; 2. a domain of crustal thinning, the Necking

556 Domain; and lastly, 3. an external distal domain interpreted to be of oceanic nature (Figure 15). No

557 transitional domain is defined in the SAB, the transition between the thinned continental and

558 oceanic crusts is direct.

559

560
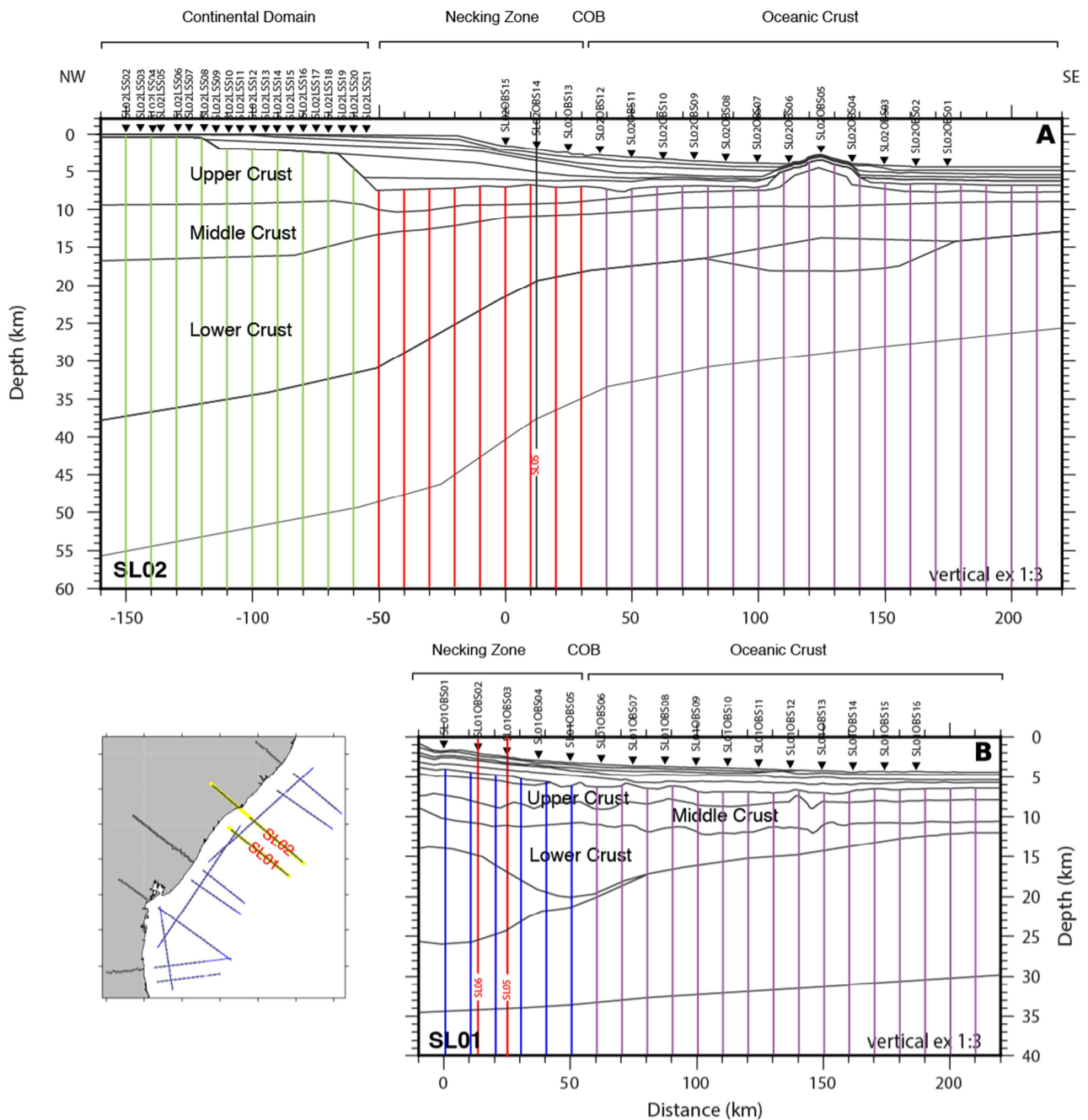
*Figure 15: Distribution of 1-D velocity profiles extracted from the final P-wave interval velocity model and color coded according to segmentation along the SL02 (A) and SL01 (B) profiles*

## Unthinned Continental Domain

This domain is essentially based on the profile SL02 data, taking into consideration that it is the unique profile with landstations.

As the inland proximal part of the profile, between the landstations and the OBSs, is not completely constrained by the seismic rays, the modeling of the Unthinned Continental domain, was also constrained by additional information obtained from the crossing with profile SL05 (Evain, *et al.,* In

28

570    prep.), and bibliographical information (Chang *et al.,* 1992 ; Feijó *et al.,* 1994 ; Mohriak *et al.,*

571    1995, 1998, 2000; Blaich *et al.,* 2008 ; Soares *et al.,* 2010 ; Tavares *et al.,* 2012 ;  de Lima *et al.,*

572    2015) .

573    In the Continental domain, the Moho is 27 to 37 km depth below basement (Figure 16). The

574    comparison of the 1D velocity profiles with a worldwide compilation of the continental crust

575    (Christensen and Mooney, 1995) clearly shows similarities both in velocities and gradients with our

576    results (Figure 16).
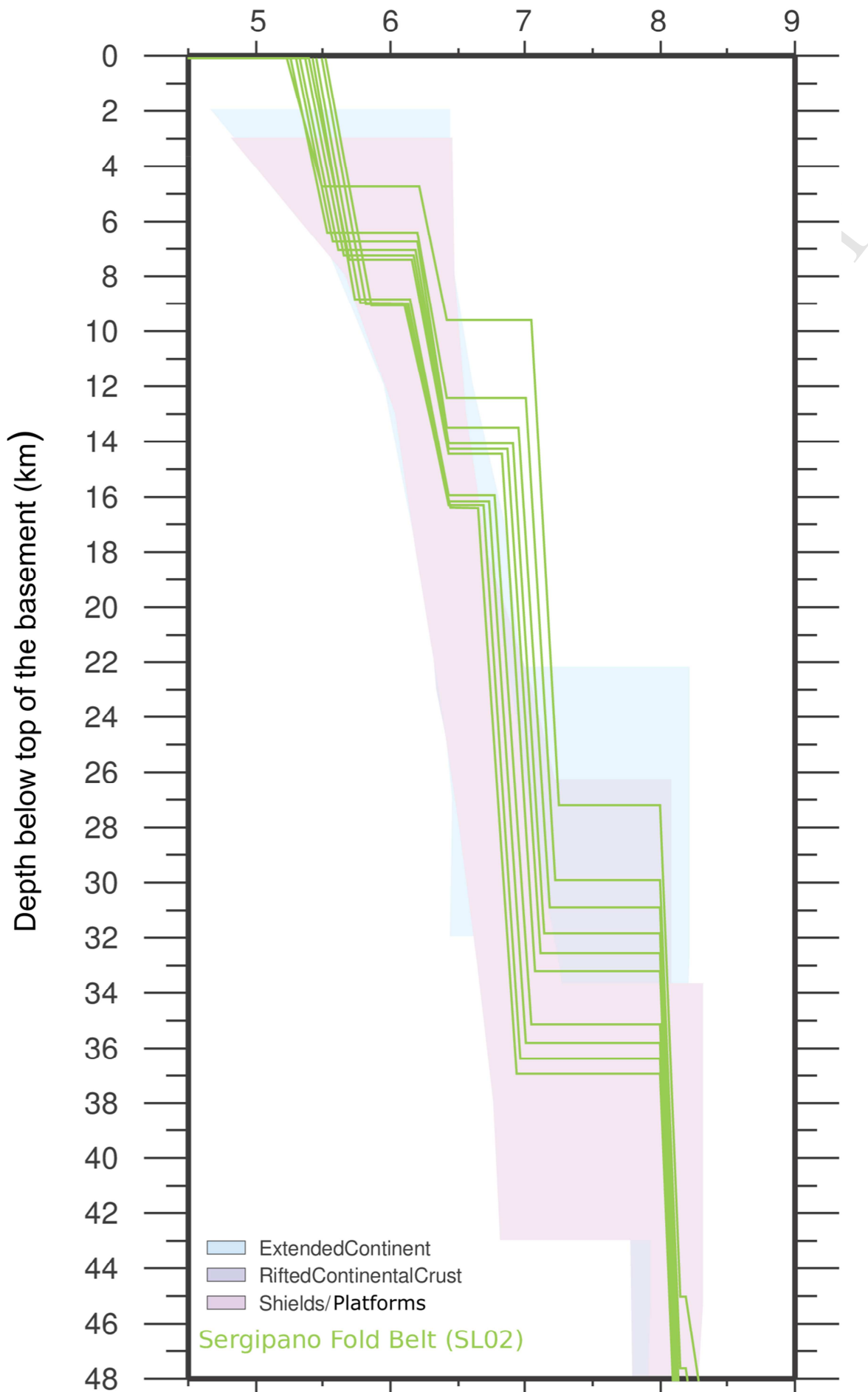
578  *Figure 16: Compilation of 1D velocity-depth profiles extracted below the top of the basement (Vz) in the domains of*

579  *unthinned continental crust. The light blue areas correspond to averaged velocity profiles for continental crust*

580  *(Christensen and Mooney, 1995).*

581

582  At the SL02 profile, in the Continental domain, the top of the upper crust, the basement, is at the

583  surface until -120 km distance model, then it deepens, forming three "stairs", first at -120 km

584  distance model, where it deepens to 2.5 km deep, and then at -60 km distance model it deepens to 8

585  km deep (Figures 15 and 16). The upper layer has velocities between 5.50 and 5.90 km/s, that

586  decreases seawards. The topography of the interface between the upper and middle crust is almost

587  regular for all along the profile, and the velocities of the middle crust range from 6.10 to 6.50 km/s.

588  The base of the lower crust corresponds to the Moho, whose depth decreases smoothly from 37 to

589  33 km. Its velocities at the top increase from 6.60 km/s in most continental part, to 7.30 km/s

590  seawards, near to the Necking Zone and its velocities at the base, range from 6.90 km/s at the

591  continental domain to 7.50 km/s near the Necking Zone.

592  The deep seismic refraction experiment carried out in the Pernambuco Province, northwards (Figure

593  1) (Soares *et al*., 2010; Tavares *et al*., 2012; Lima *et al*., 2015) shows a structure of the lithosphere,

594  with 2 layers separated at about 16 km depth, with a velocity of 5.75 to 6 km/s at the top and 6.2 to

595  6.3 km/s at the base of the upper crust, and 6.4 to 6.5 km/s at the top and 6.75 to 6.90 km/s at the

596  base of the lower crust, for a total continental crust thickness of about 32 km. In terms of velocities,

597  this structure is quite similar to that found in SL01 and SL02. The upper layer found by these

598  authors, would correspond to the upper and middle layer of SL01 and SL02.

599  These similarities put into question the proposition that the SFB is a Neoproterozoic fold–thrust belt

600  produced by inversion of a passive margin basin located at the northeastern edge of the ancient Sao

601  Francisco plate (Almeida *et al*., 1977 ; D'el-Rey Silva, 1999) and constituted by a 42 km thick crust

602  (Oliveira *et al*., 2008)  and reinforces the idea that the SFB was possibly on the margin of the

603  Palaeoproterozoic Pernambuco-Alagoas Block (Oliveira *et al.,* 2010), and was attached to the Sao

604  Francisco Craton during the Brasiliano (~600 Ma) orogenic event (Davison and Santos, 1989; Silva

605  Filho, 1998). These results put the limit clearly between the Sao Francisco Craton and the

606  Palaeoproterozoic Pernambuco-Alagoas Block on the Vaza Barris transfer zone, considering it as a

607  major structural fault.

608  **Necking Zone:**

609  The necking zone goes from -55 km to 25 km profile distance. On profile SL02, throughout the

610  necking zone, the total crustal thickness, without the water column (~4 km through the COB) and

31

611 sediment cover, thins from ~23 km to ~10 km. The thickness of the upper crust thins from 10 km in

612 the limit with the continental domain to only 1 to 2 km seaward in the limit with the oceanic

613 domain. At the depocenter of the SAB, at -50 km distance of the profile, the top of the upper crustal

614 layer deepens to ~8 km and remains at this depth for all along the profile. The thickness of the

615 middle crust thins from ~7 km in the limit with the continental domain, to ~2 km through the

616 necking domain until the COB. The Moho rises from 31 km depth in the limit with the continental

617 domain to ~18 km depth in the COB over a distance of almost 100 km (Figure 8), and the total

618 thickness of the lower crust thins from 19 km in limit with the continental domain to 8 km beneath

619 the COB, with a light velocity increase in the middle of the Necking Zone. The lateral velocity

620 change happens only in the lower crust where it changes from 7.0 to 7.3 km/s on the top and from

621 7.25 to 7.5 km/s at the base. In the Necking Zone between 30 and 90 km distance, and 9 and 15 km

622 depth, there are also packages of intra-crustal reflectors that may correspond to SDRs. Although the

623 base of the crust is much clearer in SL02 than in SL01, without basal intra-crustal reflectors.

624     The gravity data shows a prominent positive anomaly in the necking zone.

625     The necking zone of the SL01 is partially constrained in the wide-angle data (Figures 8 and

626 15), but in the MCS (Figures 4 and 14), it presents a zone of intracrustal reflectors between 4 and 8

627 km depth and between 10 and 70 km model distance. We can recognize few SDRs pattern in this

628 zone, and, in the GXT-ION profiles, a group of deeper reflectors in the lower crust, near the Moho

629 discontinuity, between 20 and 25 km depth, and between 20 and 80 km model distance. These

630 reflectors were interpreted by Mohriak *et al*. (1998) as a gradational passage from the lower crust to

631 the lithospheric mantle. In this same zone, we observe a very irregular topography in the basement,

632 showing some structures that look like volcanic plugs (Mohriak *et al.,* 1995, 1998).

633     This zone gives a chaotic response in the wide-angle data. Additionally, the fact that this area

634 is a zone with poor data coverage and no inland continuation makes difficult a detailed

635 interpretation of the crustal framework near the base of the crust. However, in wide-angle data, the

636 Pmp is very clear and allows us to make a good interpretation of the Moho discontinuity. It rises

637 from 25 km depth in the extreme NW of the profile to 18 km in the transition of the continental to

638 oceanic crust at ~70 km distance in the profile (Figure 8). In the lower crust, the array of basal intra-

639 crustal reflectors is disposed in an anticlinal pattern that gives an idea of a lenticular shape (figure

640 8). In this zone, the velocity goes from 7.0 to 7.3 km/s laterally. Loureiro *et al*. (2018) found some

641 similar structures in the profile SL11, located at the Jequitinhonha basin, near a zone of "necking

642 zone wideness" transition.

643     Buck (1991, 1999) reports "a series of basins and ranges in a broad region of continental

644 extension". According to Buck (1999), this pattern, is related to lateral periodic variations in the rate

645 of extension, which causes the so-called "lithospheric *boudinage*". This process of *boudinage* of the
646 lithosphere produces variations on the local isostasy, also called crustal buoyancy (Block and
647 Royden, 1990; Bird, 1991; Buck, 1991, 1999).

648    From the Continental Domain to seawards, the total crustal thickness, without the water
649 column (~4 km through the COB) and sediment cover, thins from ~33 km at the most continental
650 part, to ~10 km through the COB and the change in the velocity of the lower crust may therefore be
651 interpreted as a density compensation to effect of *boudinage* process and/or as volcanic intrusions.
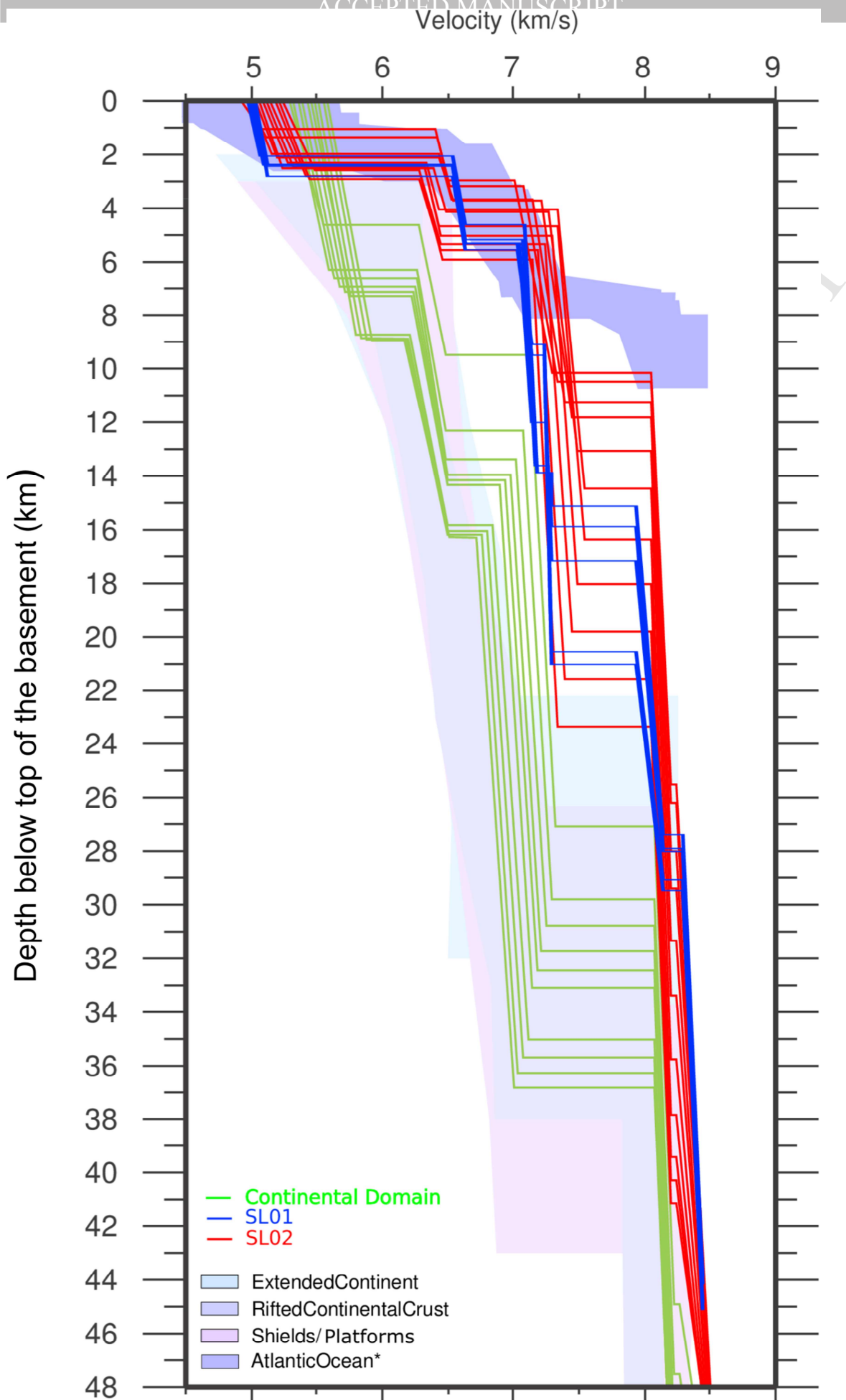
653 *Figure 17: Compilation of 1D velocity-depth profiles extracted below the top of the basement (Vz) in the Unthinned*

654 *Continental Domain (green lines) and the Necking Zone (red and blue lines). The blue shaded area bounds a*

655 *compilation of velocity profiles for typical Atlantic oceanic crust (White et al., 1992), and light blue areas correspond*

656 *to averaged velocity profiles for continental crust (Christensen and Mooney, 1995).*

657

658   Figure 17 shows that the transition between the unthinned continental crust and the thinned domain

659   preserves the configuration and the velocities of the crustal layers with strong velocity steps. The

660   total crustal thickness has a sharp transition and the comparison of the Vz of the two profiles with

661   the compilations for a typical continental crust (Christensen and Mooney, 1995) and for Atlantic-

662   type oceanic crust (White *et al.,* 1992), shows that the crustal nature in the necking zone is closer to

663   a typical continental crust than a typical oceanic crust (Figure 17). We propose that the necking

664   seems therefore to be constituted by thinned continental crust, that presents a continuity of the

665   velocity structure during the thinning process, without the presence of a transitional crust, and the

666   main change to oceanic crust occurs outside the Necking Zone.

667   **Oceanic domain:**

668   The External Domains (25-210 km distance model on SL02 and 70-210 on SL01) show a thinner

669   crustal thickness and is interpreted as formed by oceanic crust. The sedimentary cover is also

670   thinner and reaches 3 km.  The top of the basement located at 6-8 km depth assumes a much more

671   regular topography. The crustal layers do not present any significant lateral velocity gradient

672   through the transition from continental to oceanic crust. Figures 15 and 18 show that, except under

673   the volcanic edifice, where the top of the basement follows the topography of the volcano, the

674   average depth of the oceanic basement varies between 6 to 8 km (Figure 8).

675   Due to the fact that this crust was formed during the Cretaceous Normal Superchron (CNS), a

676   magnetic quiet period, it presents a lack of reversal-related magnetic anomalies on crust of age 121

677   (Anomaly M0y) to 83.6 (Anomaly C34y) Ma old (Malinverno *et al.,* 2012; Ogg, 2012; Granot *et*

678   *al.,* 2014).

679   Nevertheless, the Vz profiles (Figure 18) along the profiles SL01 and SL02 show that the oceanic

680   basement and its layers fit almost perfectly the worldwide compilation for Atlantic-type oceanic

681   crust (White *et al.,* 1992). The Moho has a range of depths below basement that varies from 6 to 12

682   km. It slightly rises from NW to SE in the proximal part of the oceanic domain (Figure 18), of the

683   closest to the transition with continental crust, and deepens under the volcanic edifice along SL02

684   profile. The rest of the oceanic crust thickness ranges from 8 to 6 km (Figure 18). Larger Moho

685   depths under the volcano can be justified due to the presence of the undercrustal layer that reflects

686     isostasy compensation. Despite the thick crust in this area, crustal velocities go according with the

687     compilation of a typical oceanic crust (White *et al.,* 1992).
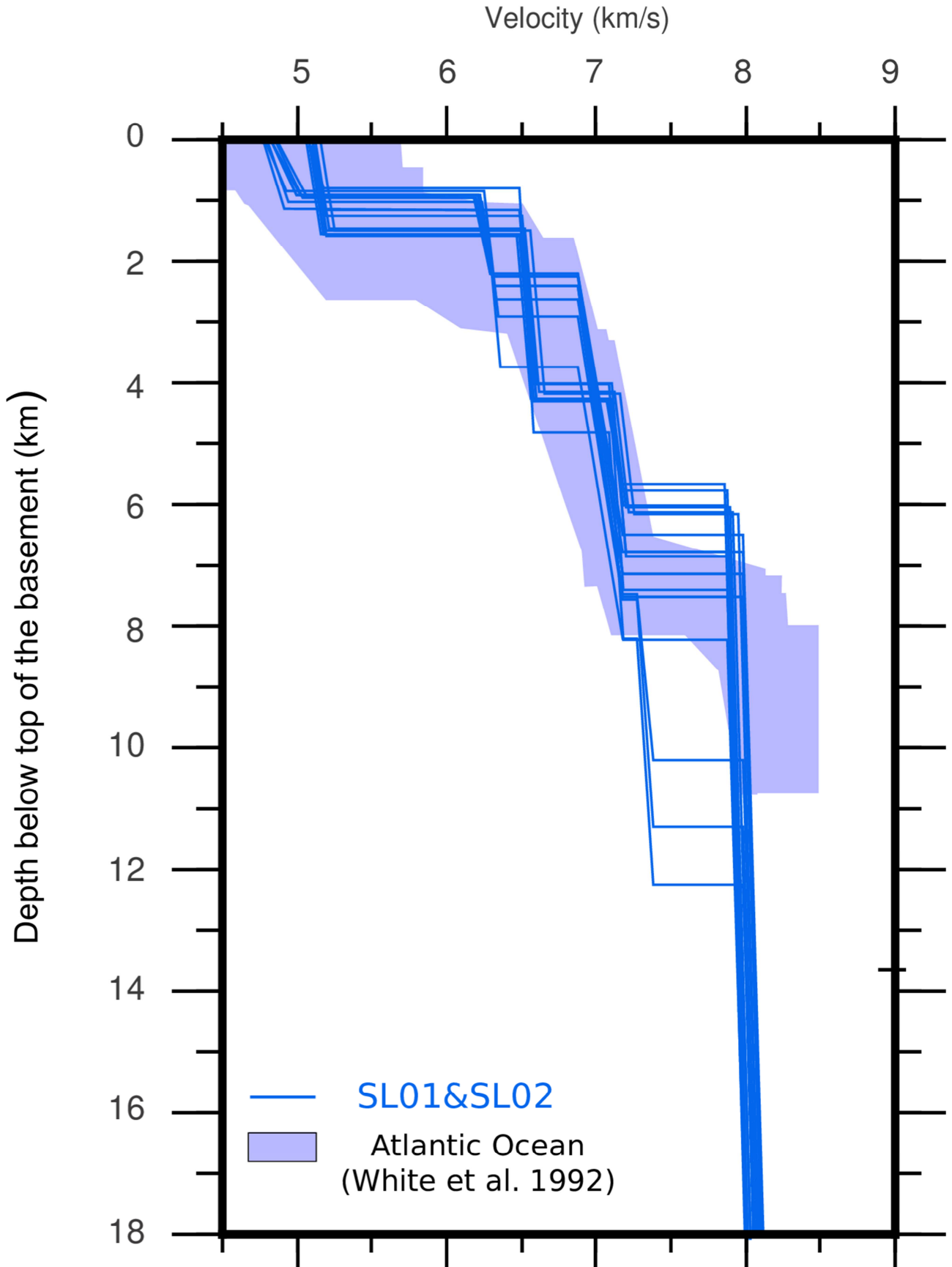
689 *Figure: 18 Compilation of 1D velocity-depth profiles extracted below the top of the basement (Vz) in the proposed*

690 *Oceanic Crust. Colored lines mark individual Vz profiles at a 10 km interval of profiles SL01 and SL02. The blue*

691 *shaded area bounds a compilation of velocity profiles for typical Atlantic oceanic crust (White et al., 1992).*

692 The figure 8 shows a comparison between the data and the segmentation obtained in this work and a

693 line-drawing of the ION-GXT seismic profiles. The wide-angle models go mostly in accord with

694 the crustal structures interpreted from the ION-GXT lines, except for the Moho along SL01 which

695 is modeled on average 2 km shallower with wide-angle data than the deepest reflector seen on the

696 depth converted MCS line.

697

698

699 **Continental-Oceanic Boundary**

700 The transition between the continental and the oceanic domain is characterized in the MCS

701 profiles (Figures 4 and 14) by a zone dominated by intracrustal reflectors. These reflectors in most

702 part look like SDRs, but there is also some that are similar to LDRs. At this zone, the basement

703 topography shows some mounds and little elevations. All these structures could be classified as a

704 magmatic signature. Notwithstanding that, as Moulin *et al.* (2005) noticed already, these structures

705 are not sufficient to characterize an archetype that could classify the margin of the SAB as a

706 volcanic margin similar to the Greenland or Argentina Margins. Moreover, there is no evidence in

707 the bibliography of volcanism before the first production of ocean crust. As described by Mohriak

708 *et al.* (1998), these magmatic features are probably associated with extensional processes and

709 oceanic crust inception, and they apparently post-date the rift phase lithospheric extension

710 associated with the breakup of Gondwana in the Early Cretaceous, and were used by Mohriak *et al.*

711 (1995, 1998) and Blaich *et al.* (2008) for their localization of the COB. Based on our wide-angle

712 data analysis, we pointed the COB at ~70 km from the coast, between the SL02OBS13 and

713 SL02OBS12 along the SL02 profile just seaward of the slight velocity increase in the lower crust,

714 and ~100 km from the coast, between the SL01OBS05 and the SL01OBS06, along the SL01 profile

715 just seaward of the intra-crustal velocity body, a little further seaward than the COB pointed by

716 these authors.

717

718 Conclusions

719 The P-wave modelling of the SL01 and SL02 profiles reveals the deep crustal structure of

720 the SAB passive margin off NE Brazil. From these models, we conclude that:

- The SAB margin is segmented parallel to the NE-SW coastline and the hinge line of the platform into a Continental Domain, a Necking Zone and an Oceanic Crust Domains without transitional domain.

- The oceanic crust is therefore rapidly reached, less than 100 km from the coast; its limit is parallel to the coast all along this segment. The COB is therefore situated a little further seaward than pointed out by Mohriak *et al*. (1995, 1998) and Blaich *et al*. (2008).

- These results show the huge segmentation in the offshore deep structures of the NE Brazilian margins since as opposed to this study a wide transitional domain of exhumed lower continental crust is imaged 350 km southwards in the Jequitinhonha margin (Loureiro *et al*., 2018).

- Onshore, LSS data along SL02 profile allow the characterization of the unthinned continental crust. It is ~30–35 km thick, divided into three layers with velocities between 5.0 and 7.2 km/s. The results confirm the general trend modelled by previous studies of Mohriak *et al*. (1995, 1998); Blaich *et al*. (2008).

- The Necking Zone presents a rather sharp crustal thinning on the north of the Vaza-Barris fault (SL02), where the Moho goes from 31 km to 18 km depth in less than 100 km, and the first thinning corresponds to the vanishing of the upper crust, that thins from 10 km, at the continental domain, to less than 2 km through the COB, and keeps this thickness seawards. The Moho rises from a depth of 33 km at the limit with Continental Domain to a depth of 16 km through the COB. The lateral velocity variation happens only in the lower crust where it goes from 7.0 to 7.3 km/s at the top and from 7.25 to 7.5 km/s at the base. This wide-angle model shows a Moho located slightly (2 km) shallower than the one found by Mohriak *et al*. (1998) and confirms the gravity model of Blaich *et al*. (2008).

- Further SE, a 9 km thick typical oceanic crust is present, with a thin upper layer (1–1.5 km) that presents velocities varying from 5.0 to 5.20 km/s, a 2.5 km thick middle layer with velocities of 6.5–6.6 km/s, and a thicker lower layer with 3-4 km thick and 6.9 to 7.1 km/s. The transition between the necking zone and this domain is characterized by a zone dominated by intracrustal reflectors, which could reflect a magmatic signature, notwithstanding that, as Moulin *et al*. (2005) noticed already, these structures are not sufficient to characterize an archetype that could classify the margin of the SAB as a volcanic margin. As described by Mohriak *et al*. (1998), these magmatic features are associated with extensional processes and oceanic crust inception, and they apparently post-date the rift phase lithospheric extension associated with the breakup of Gondwana in the Early Cretaceous.

753 • This oceanic crust is affected on profile SL02 by a volcanic edifice with 40 km

754 extension where the basement rises almost 4 km. The Bahia Seamounts chain has U/Pb ages from

755 75 to 84 Ma and is supposed to be related to a post-rift hotspot localized near the Middle Atlantic

756 Ridge (MAR) (Skolotonev, 2012). Below this domain, there is a sub-crustal layer, very well

757 constrained by the OBS and gravity data, with ~5 km thick and 7.3 km/s velocity. This layer is

758 probably related to a magmatic underplating process where basaltic magmas are frequently trapped

759 at or near the Moho, or within the crust, or in complex crust-mantle transition zones (Cox,1993).

760 • The undulated intracrustal reflectors, with an anticlinal shape, in the base of the

761 lower crust of the necking zone in SL01 profile, added to the rise in the seismic velocity are a good

762 evidence that the rift caused a lithospheric boudinage. This zone of boudinage is near of and is

763 probably affected by the Vaza-Barris Transfer Zone. A similar feature is observed further in the

764 south, at the Jequitinhonha Basin (Loureiro *et al*., 2018), where the crust is also affected by

765 boudinage, near a zone of "necking zone wideness" transition. Buck *et al*. (1999) proposed that

766 lithospheric boudinage is formed under local isostatic effect, sometimes called crustal buoyancy.

767 Due to a possible heterogeneity, the crust was affected by a non-homogeneous thinning and

768 extension, generating crustal boudinage. It can be explained by some transformations in the

769 composition of the lower crust under the necking. On the other hand, this boudinage could be a

770 consequence of  magmatic intrusions formed during the rift process. However, the Pmp in the wide-

771 angle data, is clear and continuous, and do not seem to have been influenced by a volcanic

772 intrusion.

773 • The SFB, which was in the margin of the Pernambuco Alagoas Domain, and was

774 formed by thrust faulting of this domain over the São Francisco Craton during the Brasiliano

775 orogeny, resulting in the collage of its crusts (Oliveira *et al*., 2010). The comparison between

776 velocity models of the Pernambuco Alagoas Domain (Soares *et al*., 2010; Tavares *et al*., 2012; de

777 Lima *et al*., 2015) and the São Francisco Domain (Soares *et al*., 2006 and Soares, personal

778 communication), shows that the crust in the SFB is much more similar to the Pernambuco Alagoas

779 Domain than to the São Francisco Craton. This could mean that the São Francisco crust was

780 subducted and consumed, and the crust of the Pernambuco-Alagoas predominated in the Brasiliano

781 orogenic event as it was proposed by Oliveira *et al.* (2010).

782

783 **Contributions**

784 The SALSA Project was led by D. Aslanian and M. Moulin, from Ifremer, and A. Viana and J. A.

785 Cupertino, from Petrobras. Modeling of the SALSA profile was done by M. Evain, A. Afilhado, F.

786 Gallais, A. Loureiro, F. Schnurle and F. Klingelhoefer. On-land operation was conducted by J.
787 Soares, R. Fuck, M. Vinicius de Lima, from the University of Brasilia (UnB) L. Matias, and C.
788 Corela from the Instituto Dom Luis (IDL) of the University of Lisbon. Processing of the MCS
789 seismic data was done by P. Schnurle. This work has been conducted as part of a PhD project
790 supported by the Conselho Nacional de Desenvolvimento Científico e Tecnológico (CNPQ) from
791 Brazil.

792

793 **Acknowledgments**

807 **References**

808 Almeida F. F. M., Hasui Y., Brito Neves B.B. Fuck R.A. (1977). Províncias Estruturais
809 Brasileiras. *In*: SBG-Núcleo Nordeste, Simpósio Geologia do Nordeste, 8, Campina Grande, *Atas*,
810 Boletim 6, p. 363-391.
811 Austin, J. A., Jr., and Uchupi, E. (1982). Continental-oceanic crustal transition of Southwest
812 Africa. Am. Assoc. Petrol. Geol. Bull., 66, 1328±1347
813 Bauer, K., Neben, S., Schreckenberger, B., Emmermann, R., Hinz, K., Fechner, N., Gohl, K.,
814 Schulze, A., Trumbull, R. B., Weber, K. (2000). Deep structure of the Namibia continental margin
815 as derived from integrated geophysical studies. *Journal of Geophysical Research: Solid
816 Earth*, *105*(B11), 25829-25853.
817 Blaich, O.A., Tsikalas, F., Faleide, J.I. (2008). Northeastern Brazilian margin: regional
818 tectonic evolution based on integrated analysis of seismic reflection and potential field data and
819 modelling. Tectonophysics, 458: p.51-67.
820 Blaich, O.A., Faleide, J.I. Tsikalas, F. 2011. Crustal breakup and continent-ocean transition
821 at South Atlantic conjugate margins. Journal of Geophysical Research, 116, B01402,
822 doi:10.1029/2010JB007686.

41

Black, R., and Girod, M. (1970). Late Paleozoic to Recent igneous activity in West Africa and its relationship to basement structure. *African magmatism and tectonics*, *1*(8), 5-2.

Bonatti, E. (1996). Anomalous opening of the Equatorial Atlantic due to an equatorial mantle thermal minimum. *Earth and Planetary Science Letters*, 143: 147-170.

Buck, W. R., Lavier, L. L., Poliakov, A. N. (1999). How to make a rift wide. *Philosophical Transactions-Royal Society of London Series a Mathematical Physical and Engineering Sciences*, 671-689.

Cainelli, C. (1992). Sequence stratigraphy, canyons, and gravity mass flow deposits in the Piacabuçu Formation, Sergipe-Alagoas Basin, *Brasil. PhD thesis, University of Texas at Austin*, 233 p.

Cainelli, C., and Mohriak, W. U. (1998, November). Geology of Atlantic eastern Brazilian basins. In *Brazilian Geology Part* (Vol. 2, p. 1998).

Carvalho, M. J., (2005). Tectonic Evolution of the Marancó-Poço Redondo Domain: Records of the Cariris Velhos and Brasiliano Orogenesis in the Sergipano Belt, NE Brazil. Tese de doutorado. Universidade de Campinas.

Campos Neto, O., Lima, W. S., Cruz, F. G. (2007). Bacia de Sergipe-Alagoas. *Boletim de Geociências da PETROBRAS*, *15*(2), 405-415.

Christensen, N. I., and Mooney, W. D. (1995). Seismic velocity structure and composition of the continental crust: A global view. *Journal of Geophysical Research: Solid Earth*, *100*(B6), 9761-9788. doi:10.1029/95JB00259

Cohen, J. K. and Stockwell Jr., J. W. (2010). CWP/SU: Seismic Unix Release 42: a free package for seismic research and processing, *Center for Wave Phenomena, Colorado School of Mines.*

Cornacchia, M., and Dars, R. (1983). Un trait structural majeur du continent Africain; les lineaments centrafricains du Cameroun au Golfe d'Aden. *Bulletin de la Société Géologique de France*, *7*(1), 101-109.

Conceição, J.C.J., Zalán, P.V., Wolff, S. 1988. Mecanismo, Evolução e Cronologia do Rift Sul-Atlântico, Boletim de Geociências da PETROBRAS, 2(4):255-265

Contrucci, I., Matias, L., Moulin, M., Géli, L., Klingelhofer, F., Nouzé, H., Aslanian D., Olivet J. L., Réhault J. P., Sibuet, J. C. (2004). Deep structure of the West African continental margin (Congo, Zaïre, Angola), between 5 S and 8 S, from reflection/refraction seismics and gravity data. *Geophysical Journal International*, *158*(2), 529-553.

Davison, I. and Santos, R.A., (1989). Tectonic evolution of the Sergipano Fold Belt, NE Brazil, during the Brasiliano Orogeny. Precamb. Res., 45. p. 319-342.

D'el-Rey Silva, L. J. H. (1999). Basin infilling in the southern-central part of the Sergipano Belt (NE Brazil) and implications for the evolution of Pan-African/Brasiliano cratons and Neoproterozoic sedimentary cover. *South American Journal of Earth Sciences*, *12*: 453-470

Dumont, J. F. (1986). Identification par télédétection de l'accident de la Sanaga (Cameroun): Sa position dans le contexte des grands accidents d'Afrique Centrale et de la limite nord du craton Congolais. *Géodynamique*, *1*(1), 13-19.

Eldholm, O., Thiede J., and Taylor E. (1989). Evolution of the Vøring volcanic margin, *Proceedings of the Ocean Drilling Program - Scientific Results*, 104, 1033-1065.

Feijó, F. J. (1994). Bacia de Sergipe–Alagoas. Boletim de Geociências da PETROBRAS, Rio de Janeiro, 8(1):149-161

867    Gomes, P. O. (2005). Tectonismo, Vulcanismo, Sedimentação e Processos erosivos No
868 Segmento Nordeste Da Margem Continental Brasileira. *Phd thesis. Universidade Do Estado Do Rio*
869 *De Janeiro Faculdade De Geologia*.

870    Humphrey, F. L.; Allard, G. O. (1969). Geologia da área do domo de Itabaiana (SE) e sua
871 relação com a geologia do geossinclinal de Propriá – Um elemento tectônico recem-conhecido no
872 Escudo Brasileiro. (1969). *Tradução de Munne, A. I., Barão, S. C. Rio de Janeiro,*
873 *PETROBRAS/CENPES*, 157 p. il.: mapa.

874    Klemperer, S. L., Hauge, T. A., Hauser, E. C., Oliver, J. E., Potter, C. J. (1986). The Moho in
875 the northern Basin and Range province, Nevada, along the COCORP 40 N seismic-reflection
876 transect. *Geological Society of America Bulletin*, *97*(5), 603-618.

877    Korenaga, J., Holbrook, W. S., Kent, G. M., Kelemen, P. B., Detrick, R. S., Larsen, H. C.,
878 Dahl-Jensen, T. (2000). Crustal structure of the southeast Greenland margin from joint refraction
879 and reflection seismic tomography. *Journal of Geophysical Research: Solid Earth*, *105*(B9), 21591-
880 21614.

881    Lana, M. C. (1990) Bacia de Sergipe-Alagoas: Uma Hipótese de Evolução Tectono-
882 Sedimentar. *Origem e Evolução de Bacias Sedimentares - coordenadores Raja Gabaglia, G. P. e*
883 *Milani, E. M - Petrobras/Serec/Censud,* p.311-332.

884    de Lima, M. V. A., Berrocal, J., Soares, J. E.,  Fuck, R. A. (2015). Deep seismic refraction
885 experiment in northeast Brazil: New constraints for Borborema province evolution. *Journal of*
886 *South American Earth Sciences*, *58*, 335-349.

887    Liu, Z., Bleistein, N. (1995). Migration velocity analysis: Theory and an iterative
888 algorithm. *Geophysics*, *60*(1), 142-153.

889    Ludwig W.J., Nafe J.E.  Drake L.E. (1970). Seismic refraction. Maxwell, A.E. (Editor), *The*
890 *Sea. New concepts of sea floor evolution*. Wiley-Interscience, New York, 4(I): 53-84.

891    Lutter, W. J., Nowack, R. (1990). Inversion for crustal structure using reflections from the
892 PASSCAL Ouachita experiment. *Journal of Geophysical Research: Solid Earth*, *95*(B4), 4633-
893 4646.

894    Mohriak, W.U., Rabelo, J.H.L., Matos, R.D., Barros, M.C. (1995). Deep Seismic Reflection
895 Profiling of Sedimentary Basins offshore Brazil: Geological Objectives and Preliminary Results in
896 the Sergipe Basin. *Journal of Geodynamics, 20:*515-539

897    Mohriak, W.U., Bassetto, M. Vieira, I.S. (1998). Crustal Architecture and Tectonic Evolution
898 of the Sergipe–Alagoas and Jacuípe Basins, Offshore Northeastern Brazil. *Tectonophysics,*
899 *288*:199-220.

900    Mohriak, W.U., Mello, M.R., Bassetto, M., Vieira, I.S., Koutsoukos, E.A.M. (2000). Crustal
901 architecture, sedimentation, and petroleum systems in the Sergipe–Alagoas Basin, Northeastern
902 Brazil. *In*: Mello, M.R., Katz, B.J. (eds.). *Petroleum systems of South Atlantic margins, AAPG*
903 *Memoir 73:*273-300

904    Mohriak, W. U. (2003). Bacias sedimentares da margem continental Brasileira. *Geologia,*
905 *tectônica e recursos minerais do Brasil*, *3*, 87e165.

906    Moulin, M., D. Aslanian, J.-L. Olivet, I. Contrucci, L. Matias, L. Géli, F. Klingelhoefer, H.
907 Nouzé, J.-P. Réhault, and P. Unternehr (2005). Geological constraints on the evolution of the
908 Angolan margin based on reflection and refraction seismic data (ZaïAngo project). *Geophysical*
909 *Journal International*, *162*(3), 793-810.

910    Moulin, M., D. Aslanian, and P. Unternehr (2010), (2010). A new starting point for the South
911 and Equatorial Atlantic Ocean. *Earth-Science Reviews*, *98*(1-2), 1-37.

912       Oliveira, D.C., Windley, B.F., Araújo, D.B. (2010). The Neoproterozoic Sergipano orogenic
913 belt, NE Brazil: A complete plate tectonic cycle in western Gondwana. *Precambrian Research 181,*
914 64-84.

915       Oliveira, R. G. D. (2008). Arcabouço geofísico, isostasia e causas do magmatismo cenozóico
916 da Província Borborema e de sua margem continental (Nordeste do Brasil).

917       Pavlis, N. K., Holmes, S. A., Kenyon, S. C., Factor, J. K. (2012). The development and
918 evaluation of the Earth Gravitational Model 2008 (EGM2008). *Journal of Geophysical Research:*
919 *Solid Earth*, *117*(B4).

920       Sandwell, D. T., Müller, R. D., Smith, W. H., Garcia, E., Francis, R. (2014). New global
921 marine gravity model from CryoSat-2 and Jason-1 reveals buried tectonic
922 structure. *Science*, *346*(6205), 65-67.

923       Sandwell, D., Smith, W. (1997). Marine gravity anomaly from GEOSAT and ERS-1 satellite
924 altimetry. *Journal of Geophysical Research, 102:10.039-*10.054.

925       Santos, E. D., Silva Filho, M. A. (1975). Ensaio interpretativo sobre as evolução da
926 Geossinclinal de Propriá, Nordeste do Brasil. *Revista Mineração e Metalurgia*, *367*, 3-22.

927       Schaller, H. (1970). Revisão estratigráfica da bacia Sergipe-Alagoas. Boletim Técnico da
928 Petrobrás. 12 (1): 21-86

929       Skolotnev S. G., Bylinskaya M. E, Golovina L. A., and Ipat'eva I. S. (2012). The Origin of
930 Bahia Seamounts (Brazil Basin, South Atlantic) in Connection to New Data on Their Age. *Doklady*
931 *Earth Sciences, 2012, Vol. 443, Part 2, pp. 444–450. ISSN 1028_334X.*

932       Silva Filho, M. A., (1998). Arco vulcânico Canindé-Marancó e a Faixa Sul-Alagoana:
933 sequências orogênicas Mesoproterozóicas. In: XL *Congresso Brasileiro de Geologia, Belo*
934 *horizonte, SBG.* p. 16.

935       Soares J.E.P., Berrocal J., Fuck R.A., Mooney W.D.  Ventura D.B.R. (2006). Seismic
936 characteristics of central Brazil crust and upper mantle: A deep seismic refraction study. *Journal of*
937 *Geophysical Research*, 111: 1-31.

938       Soares, J. E. P., de Lima, M. V., Fuck, R. A., Berrocal, J. (2010). Características sísmicas da
939 litosfera da Província Borborema: Resultados parciais do experimento de refração sísmica profunda.
940 In *IV Simpósio Brasileiro de Geofísica*.

941       Stockwell, J. W., Jr. (1999), The CWP/SU: Seismic Un x package, Comput. Geosci., 25(4),
942 415–419, doi:10.1016/S0098-3004(98)00145-9.

943       Szatmari, P. (1998). Tectonic habitat of petroleum along the South Atlantic margins. In Am.
944 Assoc. Petrol. Geol. *International Conference Extended Abstracts Volume, Rio de Janeiro, Brazil,*
945 pp. 362±363.

946       Szatmari, P., Milani, E.J. (1999). Microplate rotation in northeast Brazil during South Atlantic
947 rifting: analogies with the Sinai microplate. Geology, 27(12):1115-1118

948       Tard F., Masse P., Walgenwitz F., Gruneisen P., The volcanic passive margin in the vicinity
949 of Aden, Yemen, Bulletin des centres de recherche et d'exploration-production Elf-Aquitaine 15
950 (1991) 1–9

951       Tavares, E. J., Soares, J. E. P., Fuck, R. A.,  De Lima, M. V. A. (2012). Modelagem de onda P
952 e razão Vp/Vs da crosta sob a linha de refração sísmica profunda NW-SE da Província Borborema.
953 In *V Simpósio Brasileiro de Geofísica*.

954       White, R. S., McKenzie, D. and O'Nions, R. K. (1992). Oceanic crustal thickness from
955 seismic measurements and rare earth element inversions. *Journal of Geophysical Research: Solid*
956 *Earth*, *97*(B13), 19683-19715. doi:10.1029/92JB01749.

957    Zelt, C. A. (1999), Modelling strategies and model assessment for wide angle seismic
958    traveltime data, *Geophysical Journal International*, *139*, 183–204.

959

960

961

962

963

964

965

966

967

968

969

970

971

972

973